1   **Title:** New fossils from Jebel Irhoud (Morocco) and the Pan-African origin of *Homo*

2   *sapiens.*

3

4   Jean-Jacques Hublin[1]

5   Abdelouahed Ben-Ncer[2]

6   Shara E. Bailey[3]

7   Sarah E. Freidline[1]

8   Simon Neubauer[1]

9   Matthew M. Skinner[4]

10   Inga Bergmann[1]

11   Adeline Le Cabec[1]

12   Stefano Benazzi[5]

13   Katerina Harvati[6]

14   Philipp Gunz[1]

15

16   [1] Department of Human Evolution, Max Planck Institute for Evolutionary Anthropology,

17   Deutscher Platz 6, Leipzig, 04103, Germany

18   [2] Institut National des Sciences de l'Archéologie et du Patrimoine, Rabat, Morocco

19   [3] Department of Anthropology, Center for the Study of Human Origins, New York

20   University, New York, NY 10003, USA

21   [4] School of Anthropology and Conservation, University of Kent, Canterbury CT2 7NR,

22   United Kingdom

23   [5] Department of Cultural Heritage, University of Bologna, Ravenna 48121, Italy

24   [6]Paleoanthropology, Senckenberg Center for Human Evolution and Paleoenvironment,

25   and DFG Center for Advanced Studies: "Words, Bones, Genes, Tools", Eberhard Karls

26   Universität, Tübingen, Germany

Fossil evidence points to an African origin of *Homo sapiens* from a group called either *H. heidelbergensis* or *H. rhodesiensis*. However, the exact place and time of our species' emergence remain obscure because the fossil record is scarce and the chronological age of many key specimens remains uncertain. In particular, it is unclear whether the present day "modern" morphology emerged rapidly ca. 200 thousand years ago (ka) among earlier representatives of *H. sapiens* [1] or evolved gradually over the last 400 ka[2]. Here, we report on new human fossils from Jebel Irhoud (Morocco), and interpret the affinities of the hominins from this site with other archaic and recent human groups. We identified a mosaic of features including a facial, mandibular and dental morphology that aligns the Jebel Irhoud material with early (EMH) or recent anatomically modern humans (RMH) and a more primitive neurocranial and endocranial morphology. In combination with the new date of 300-350 ka[3], this evidence makes Jebel Irhoud the oldest and richest African Middle Stone Age hominin site documenting early stages of the *H. sapiens* clade in which key features of modern morphology were established. Furthermore, it shows that the evolutionary processes behind the emergence of our species were not restricted to sub-Saharan Africa.

In 1960, mining operations in the Jebel Irhoud massif 55 km southeast of Safi, Morocco exposed a Palaeolithic site in the Pleistocene filling of a karstic network. An almost complete skull (Irhoud 1) was accidentally unearthed in 1961, prompting excavations that yielded an adult braincase (Irhoud 2)[4], an immature mandible (Irhoud 3)[5], an immature humeral shaft[6], an immature ilium[7] and a fragment of mandible[8] associated with abundant faunal remains and Levallois stone tool technology[6]. Although these

51   human remains were all reported to come from the bottom of the archaeological

52   deposits, only the precise location of the humeral shaft was recorded.

53

54   The interpretation of the Irhoud hominins has long been complicated by persistent

55   uncertainties surrounding their geological age. They were initially assigned to a time

56   period ca. 40 ka ago and considered to be an African form of Neanderthal[9]. However,

57   these affinities have been challenged[5,10,11] and the faunal[8] and microfaunal[12] evidence

58   supported a middle Pleistocene (MP) age for the site. An attempt to date one of the

59   hominins directly by U series-ESR[3] suggested an age of 160 ± 16 ka[13]. Consistent with

60   some genetic evidence[14], fossils from Ethiopia (Omo Kibish, considered to be as old as

61   ~195 ka[15] and Herto, dated to ~160[16] ka) are commonly regarded as the first EMH.

62   Intriguingly, Omo 1 and the Herto specimens appear to be more derived than the

63   supposedly contemporaneous or even younger Irhoud hominins. It has therefore been

64   suggested that the archaic features of the Irhoud fossils may indicate that North African

65   *H. sapiens* interbred with Neanderthals[17], or that the Irhoud hominins represented a

66   North African, late surviving, archaic population[18].

67

68   New excavations at Irhoud have recovered *in situ* archaeological material and

69   established a precise chronology for the deposits, which are much older than previously

70   thought[3]. The excavation yielded a new series of hominin remains, including an adult

71   skull (Irhoud 10) comprising of a distorted braincase and fragments of the face (Fig. 1), a

72   nearly complete adult mandible (Irhoud 11) (Fig. 2), one maxilla, several postcranial

73   elements, and abundant dental material (Extended Data Table 1). These remains

74   primarily come from a single bone bed in the lower part of the archaeological deposits.

75   This concentration, stratigraphical observations made by previous excavators, and the

76   anatomical similarity with earlier discoveries strongly suggest that most, if not all, of the

77   hominin remains from the site were accumulated in a rather constrained window of

78   time corresponding to the formation of layer 7. This layer contains the remains of at

79   least five individuals (three adults, one adolescent and one immature, ca. 7.5 years old).

80   It now has a thermoluminescence (TL) weighted average age between 300 and 350 ka

81   with a 95 % probability, compatible with a series of newly established U series-ESR

82   dates[3]. This timeframe places the Irhoud evidence in an entirely new perspective.

83

84   **Facial and mandibular morphology**

85   When compared to the large, robust and prognathic faces of the Neanderthals or older

86   MP forms, the facial morphology of EMH and RMH is very distinctive. The face is

87   relatively short and retracted under the braincase. Facial structures are coronally

88   oriented and the infraorbital area is of "inflexion-type", displaying curvatures along the

89   horizontal, sagittal and coronal profiles. This pattern, which may include some primitive

90   retentions[19], strongly influences the morphology of the maxilla and zygomatic bone. Our

91   morphometric analysis (Fig. 3 and Methods) clearly distinguishes MP archaic humans

92   and Neanderthals from RMH. In contrast, all the possible reconstructions of the new

93   facial remains of Irhoud 10 fall well within RMH variation, as does Irhoud 1.

94

95   Another facial characteristic observed in RMH is the weakness of their brow ridges.

96   Some EMH from Africa and the Levant still display protruding supraorbital structures,

97   but they tend to be dissociated into a medial superciliary arch and a lateral supraorbital

98   arch. Among the Irhoud hominins these structures are rather variable, which may be

99   related to sexual dimorphism. Irhoud 1 displays protruding supraorbital structures and

100 the arches are poorly separated. However in frontal view, the supraorbital buttress

101 tends to form an inverted V above each orbit. On Irhoud 2, the torus is less projecting

102 and a modern pattern is already well expressed, with a clear sulcus separating the two

103 arches. On Irhoud 10, the preserved parts do not display projecting supraorbital

104 structures (Fig. 1).

105

106 The new Irhoud 11 mandible is very large overall (Fig. 2, Extended Data Table 2). As in

107 some EMH from the Levant or North Africa, it has retained a vertical symphysis, with a

108 mental angle of 88.8° (Extended Data Fig. 1). The mandibular body displays a pattern

109 typical of *H. sapiens*: its height strongly decreases from the front to the back. This feature

110 is also present on the immature individual Irhoud 3. Another modern aspect of Irhoud

111 11 is the rather narrow section of the mandibular body expressed by the breadth/height

112 index at the level of the mental foramen (Extended Data Fig. 1). The Irhoud mandibles

113 also display some derived conditions in the mental area (Extended Data Fig. 1). The

114 symphyseal section of Irhoud 11 has a tear-shaped outline quite distinctive of our

115 species. Although the Irhoud mandibles lack a marked mandibular incurvation, the

116 juvenile Irhoud 3 displays a central keel between two depressions expanding inferiorly

117 into a thickened triangular eminence. This inverted T-shape, typical of recent *H.*

118 *sapiens*[20], is incipient on the adult. Its inferior border is somewhat distended and

119 includes separated tubercles. Notably, this modern pattern is still inconsistently present

120 on Levantine EMH[20]. In some aspects, Irhoud 11 is evocative of the Tabun 2 mandible,

121 but is much more robust.

122

123 **Dental morphology**

124 The Irhoud teeth are generally very large (Extended Data Tables 3 and 4). However,

125 their dental morphology is reminiscent of EMH in several respects. The anterior teeth do

126   not display the expansion observed in non-*sapiens* MP hominins and Neanderthals[21] and

127   the postcanine teeth are reduced compared to older hominins. The M^3 of the Irhoud 21

128   maxilla is already smaller than in some EMH. The crown morphology (Extended Data

129   Table 5 and Extended Data Fig. 2) also aligns the Irhoud specimens most closely with *H.*

130   *sapiens,* rather than with non-*sapiens* MP hominins and Neanderthals. They do not

131   display expanded and protruding M^1 hypocones, lower molar middle trigonid crests

132   (especially at the EDJ), or a P_4 with a transverse crest, uninterrupted by a longitudinal

133   fissure. The molars are morphologically complex and reminiscent of large-toothed

134   African EMH, possessing accessory features such as cusp 6, cusp 7 and protostylid on the

135   lower molars and cusp 5 on the upper molars. The enamel-dentine junction analysis

136   demonstrates the retention of a non-Neanderthal primitive pattern of the P_4 (Extended

137   Data Fig. 2b). However, derived crown shapes shared with RMH are already expressed

138   on the upper and lower molars, grouping Irhoud 11 with EMH from North Africa and the

139   Levant. The lower incisor and canine roots retain a large size, but the shape is already

140   within the range of the modern distribution (Extended Data Fig. 3). Mandibular molar

141   roots are cynodont, i.e. modern human-like. This mandibular root configuration of

142   Irhoud 11 is similar to that observed in EMH from Qafzeh. Finally, Irhoud 3 shows a

143   pattern of eruption and a period of dental development close to recent *H. sapiens*[13].

144

145   **Neurocranium**

146   In contrast to their modern facial morphology, the Irhoud crania retain a rather

147   primitive overall shape of the braincase and endocast, i.e. unlike those of RMH, they are

148   elongated and not globular [10,18,22]. This is expressed in a low outline of the occipital

149   squama, elongated temporal bones and a low convexity of the parietal[11]. However, the

150   frontal squama displays a rather vertical orientation and a marked convexity when

151   compared to that of archaic MP specimens. These derived conditions are especially well

152   expressed on Irhoud 2[11]. A geometric morphometric analysis (Extended Data Fig. 4) of

153   external vault shape distinguishes Neanderthals and archaic MP forms with their

154   primitive neurocranial shape from RMH and Upper Palaeolithic Humans. With regards

155   to PC 1, Irhoud 1 and 2 are intermediate and group together with specimens such as

156   Laetoli H18 and Qafzeh as well as Upper Palaeolithic individuals from Mladeč or

157   Zhoukoudian Upper Cave. To some degree all these specimens retained longer and

158   lower braincase proportions compared to RMH.

159

160   The morphometric analysis of endocranial shape (Fig. 3b), which is not affected by

161   cranial superstructures, shows a clear separation between *H. erectus* and the

162   Neanderthal/archaic MP cluster along PC 2. The latter have evolved larger neocortices

163   but, in contrast to RMH, without proportional increase of the cerebellum (Extended Data

164   Fig. 5). EMH and the Irhoud hominins also display elongated endocranial profiles, but

165   are intermediate between *H. erectus* and the cluster of Neanderthals /archaic MP

166   hominins along PC2. They range in rough agreement with their geological age along PC1,

167   in a morphological cline ending with extant globular brain shapes of RMH. Notably, Omo

168   2 falls between Irhoud 1 and 2. This similarity re-opens the question of the

169   contemporaneity of Omo 1 and 2[23] but also raises the possibility of a late evolution of

170   modern brain shape in the *H. sapiens* clade.

171

172   **Conclusion**

173   The Irhoud fossils currently represent the most securely dated evidence of the early

174   phase of *Homo sapiens* evolution in Africa, and they do not simply appear as

175   intermediate between African archaic MP forms and RMH. Even ca. 300-350 ka ago their

176   facial morphology is almost indistinguishable from that of RMH, corroborating the

177   interpretation of the fragmentary specimen from Florisbad (South Africa) as a primitive

178   *H. sapiens* tentatively dated to 260 ka[24]. Anatomical mandibular and dental features, as

179   well as developmental patterns also align them with EMH. Importantly, the endocast

180   analysis suggests diverging evolutionary trajectories between early *H. sapiens* and MP

181   archaic African forms. This anatomical evidence and the chronological proximity

182   between the two groups[25] reinforce the hypothesis of a rapid anatomical shift or even, as

183   suggested by some[26], of a chronological overlap.

184

185   The Irhoud evidence supports a complex evolutionary history of our species involving

186   the whole African continent[25,27]. Like in the Neandertal lineage[28], facial morphology was

187   established early on, and evolution in the last 300 ka primarily affected the braincase.

188   This likely occurred in relation to a series of genetic changes affecting brain

189   connectivity[29], organization and development[22]. Through accretional changes, the

190   Irhoud morphology is directly evolvable into that of extant humans. Delimiting clear-cut

191   anatomical boundaries for a "modern" grade within the *H. sapiens* clade thus only

192   depends on gaps in the fossil record[30].

References.

1   Stringer, C. Modern human origins: progress and prospects. *Phil. Trans. R. Soc. Lond. B* **357**, 563-579 (2002).
2   Bräuer, G. The origin of modern anatomy: by speciation or intraspecific evolution? *Evolutionary Anthropology* **17**, 22-37 (2008).
3   Richter, D. *et al. The Age of the Homo sapiens fossils and Middle Stone Age artefacts from Jebel Irhoud, Morocco* (2016). Manuscript submitted for publication.
4   Ennouchi, E. Le deuxième crâne de l'homme d'Irhoud. *Annales de Paléontologie (Vértébrés)* **LIV**, 117-128 (1968).
5   Hublin, J.-J. & Tillier, A. M. The Mousterian Juvenile Mandible from Irhoud (Morocco): A Phylogenetic Interpretation. in *Aspects of Human Evolution* Vol. 21 *Symposia of the Society for the study of Human Biology, Volume XXI* (ed C.B. Stringer) 167-186 (Taylor & Francis Ltd., 1981).
6   Hublin, J. J., Tillier, A. M. & Tixier, J. L'humerus d'enfant moustérien (Homo 4) du Jebel Irhoud (Maroc) dans son contexte archéologique. *Bulletins et Mémoires de la Société d'Anthropologie de Paris* **4**, 115-142 (1987).
7   Tixier, J., Brugal, J.-P., Tillier, A.-M., Bruzeket, J. & Hublin, J.-J. Irhoud 5, un fragment d'os coxal non adulte des niveaux mousteriens marocains. in *Actes des 1ères Journées Nationales d'Archéologie et du Patrimoine. Volume 1: Préhistoire* Vol. 1 149-153 (Société Marocaine d'Archéologie et du Patrimoine, 2001).
8   Amani, F. & Geraads, D. Le gisement moustérien du Djebel Irhoud, Maroc: précisions sur la faune et la biochronologie, et description d'un nouveau reste humain. *Comptes Rendus à l'Académie des Sciences de Paris* **316**, 847-852 (1993).
9   Ennouchi, E. Un Néanderthalien: l'homme du Jebel Irhoud (Maroc). *L'anthropologie* **66**, 279-299 (1962).
10   Stringer, C. B. Some problems in middle and upper Pleistocene hominid relationship. in *Recent advances in Primatology.* (eds D.J. Chivers & K.A. Joysey) 395-418 (Academic Press, 1978).
11   Hublin, J.-J. Recent human evolution in Northwestern Africa. *Phil. Trans. R. Soc. Lond.* **B337**, 185-191 (1992).
12   Geraads, D. *et al.* The rodents from the late middle Pleistocene hominid-bearing site of J'bel Irhoud, Morocco, and their chronological and paleoenvironmental implications. *Quaternary Research* **80**, 552-561 (2013).
13   Smith, T. M. *et al.* Earliest evidence of modern human life history in North African early *Homo sapiens. Proceedings of the National Academy of Sciences of the USA* **104** (2007).
14   Gonder, M. K., Mortensen, H. M., Reed, F. A., de Sousa, A. & Tishkoff, S. A. Whole-mtDNA Genome Sequence Analysis of Ancient African Lineages. *Molecular Biology and Evolution* **24**, 757-768 (2007).

15   McDougall, I., Brown, F. H. & Fleagle, J. G. Stratigraphic placement and age of modern humans from Kibish, Ethiopia. *Nature* **433**, 733-736 (2005).
16   White, T. D. *et al.* Pleistocene *Homo sapiens* from Middle Awash, Ethiopia. *Nature* **423**, 742-747 (2003).

17   Smith, F. H. The role of continuity in modern human origins. in *Continuity or replacement, controversies in Homo sapiens evolution*   (eds Günter Bräuer & Fred H. Smith) 145-156 (A. A. Balkema, Zagreb, 1992).

18   Bruner, E. & Pearson, O. Neurocranial evolution in modern humans: the case of Jebel Irhoud 1. *Anthropological Science* **121**, 31 (2013).

19   Bermúdez de Castro, J.M., Arsuaga, J.L., Carbonell, E., Rosas, A., Martinez, I., Mosquera, M., A hominid from the Lower Pleistocene of Atapuerca, Spain: possible ancestor to Neandertals and modern humans *Science*, **276,** ,1392-1395 (1997).

20   Schwartz, J. H. & Tattersall, I. The human chin revisited: what is it and who has it? *Journal of Human Evolution* **38**, 367-409 (2000).

21   Trinkaus, E. Dental Remains from the Shanidar Adult Neanderthals. *J Hum. Evol.* **7,** 369-382 (1978)

22   Gunz, P. *et al.* A uniquely modern human pattern of endocranial development. Insights from a new cranial reconstruction of the Neandertal newborn from Mezmaiskaya. *Journal of Human Evolution* **62**, 300-313 (2012).

23   Klein RG. *The human career: human biological and cultural origins* (third edition). Chicago: University of Chicago Press. (2009).

24   Grün, R. *et al.* Direct dating of Florisbad hominid. *Nature* **382**, 500-501 (1996).

25   Stringer, C. *The origin of our species.* (Allen Lane - Penguin Books, 2011).

26   Harvati, K. *et al.* The Later Stone Age Calvaria from Iwo Eleru, Nigeria: Morphology and Chronology. *PLoS ONE* **6**, e24024, (2011).

27   Gunz, P. *et al.* Early modern human diversity suggests subdivided population structure and a complex out-of-Africa scenario. *Proceedings of the National Academy of Sciences of the United States of America* **106**, 6094-6098 (2009).

28   Arsuaga J.L. *et al*. Neandertal roots: Cranial and chronological evidence from Sima de los Huesos. *Science* **344**, 1358-1363 (2014)

29   Meyer, M. *et al.* A High-Coverage Genome Sequence from an Archaic Denisovan Individual. *Science* **338**, 222-226, (2012).

30   Weaver, T. D. Did a discrete event 200,000–100,000 years ago produce modern humans? *Journal of Human Evolution* **63**, 121-126, (2012).

METHODS

Computed tomography

The original fossil specimens were scanned using a BIR ARCTIS 225/300 industrial micro-CT scanner, at the Max Planck Institute for Evolutionary Anthropology (MPI EVA), Leipzig, Germany. The non-dental material was scanned with an isotropic voxel size ranging from 27.4 to 91.4 μm (130 kV, 100 to 150 μA, 0.25 to 2.0 mm brass filter, 0.144 degree of rotation step, 2 to 3 frames averaging, 360 degrees of rotation). The dental material was scanned with an isotropic voxel size ranging from 12.8 to 32.8 μm (130 kV, 100 μA, 0.25 to 0.5 mm brass filter, 0.144 degree of rotation step, 3 frames averaging, 360 degrees of rotation). Segmentation of the micro-CT volume was performed in Avizo (Visualization Sciences Group). The comparative dental sample was scanned with an isotropic voxel size ranging from 11.6 to 39.1 μm at the MPI EVA on a BIR ARCTIS 225/300 micro-CT scanner (130 to 180 kV, 100 to 150 μA, 0.25 to 2.0 mm brass filter, 0.096 to 0.144 degree of rotation step, 2 to 4 frames averaging, 360 degrees of rotation) or on a Skyscan 1172 micro-CT scanner (100 kV, 100 μA, 0.5 mm aluminum and 0.04 mm copper filters, 0.10 to 1.25 degree of rotation step, 360 degrees of rotation, 2 to 4 frames averaging). The micro-CT slices were filtered using a median filter followed by a mean-of-least-variance filter (each with a kernel size of three) to reduce the background noise while preserving and enhancing edges[31].

Virtual Reconstruction

Using Avizo, nine reconstructions of the Jebel Irhoud 10 face were made based on segmented surfaces of its preserved parts consisting of a left supraorbital torus, two left maxillary fragments and a nearly complete left zygomatic bone. First, we used several recent modern humans from diverse geographical regions (e.g., Africa, North America and Australia) and Irhoud 1 as a reference to align the two left maxillary bones. Since a large portion of the dental arcade of Irhoud 10 is preserved, the range of possible "anatomically correct" alignments in the palate was limited (Figure 1b). Based on this maxillary alignment, each of the subsequent reconstructions differed by several millimeters in the following ways: broadening the palate; increasing the facial height; increasing the orbital height; or rotating the zygomatic bones anteriorly or posteriorly in a parasagittal direction. Additionally, we aligned one reconstruction to match the facial proportions and orientation of a "classic" Neanderthal (La Ferrassie 1). In doing so, the zygomatic bone

was rotated parasagittally and moved posteriorly (> 5 mm). Correspondingly, the brow ridge was realigned postero-superiorly by several mm, and the maxillary bones were moved inferiorly several mm to increase its facial height. For each reconstruction, each bone was mirror-imaged along the mid-sagittal plane of Irhoud 1 and then the right and left sides were merged to form one surface model. The reconstruction of the Irhoud 11 mandible was conducted by mirroring the left side of the mandible, which was best preserved and minimally distorted, onto the right side, apart from the condyle, which was only preserved on the right side and mirrored onto the left side. The left side of the mandible was represented by three main fragments. Before mirroring, the sediment filling the cracks between the main fragments was virtually removed, the fragments were re-fitted and the broken crown of the left canine was reset on its root. Note that the position of the condyles in the reconstruction is only indicative.

Shape analysis of the face, endocast and cranial vault

Geometric morphometric methods (GMM) were used to analyse different aspects of morphology of the Irhoud fossils in a comparative context. To this end we digitised three-dimensional landmarks and sliding semilandmarks[32, 33, 34]to separately analyse the shape of the face, the endocranial profile and the external vault. On the face (Figure 3a), 3D coordinates of anatomical landmarks, as well as curve and surface semilandmarks (n=791) were digitized using Landmark Editor[35] either on CT scans (BIR ACTIS 225/300 and Toshiba Aquilion), or surface scans (Minolta Vivid 910 and Breuckmann optoTOP-HE) of recent modern human and fossil crania (n =267) following Freidline *et al.*[36]. Whenever possible, measurements were taken on scans of the original fossil; landmarks on some fossil specimens were measured on scans of research-quality casts. Avizo was used to extract surface files from the CT scans; data from surface scanners were pre-processed using Geomagic Studio (Geomagic Inc.) and OptoCat (Breuckmann). On the endocast (Fig. 3b), landmarks and semilandmarks (n =31) along the internal midsagittal profile of the braincase were digitised on CT scans of the original specimens (n =86) in Avizo (Visualization Sciences Group) following the measurement protocol described in Neubauer *et al.*[37], and converted to two-dimensional data by projecting them onto a least squares plane in Mathematica (Wolfram Research). On the external vault (Extended Data Fig. 4), coordinate measurements of 97 anatomical landmarks and curve semilandmarks (along the external midsagittal profile from glabella to inion, the coronal and lambdoid

sutures, and along the upper margin of the supraorbital torus) were captured using a Microscribe 3DX (Immersion Corp.) portable digitiser on recent and fossil braincases (*n* =296) following the measurement protocol described in Harvati *et al.*[38]. The points along sutures were later resampled automatically in Mathematica to ensure the same semilandmark count on every specimen.

Homo erectus samples include KNM ER 3733 (3733), KNM ER 3883 (3883), KNM WT 15000. MP archaic samples include Petralona (Petr), Arago, Sima de los Huesos H5 (SH5), Saldanha, Kabwe, Bodo. Neanderthal samples include La Chapelle-aux-Saints 1 (LaCha), Guattari 1 (Guatt), La Ferrassie 1 (LF 1), Forbes' Quarry 1 (Gibr), Feldhofer (Feld), La Quina 5 (LQ 5), Spy 1 and 2 (Sp 1, Sp 2), Amud 1 (Amud), Shanidar 1 and 5 (Shan 1, Shan 5). Primitive *H. sapiens* and EMH include Laetoli H18 (LH), Omo Kibish 2 (Omo 2), Singa (Si), Qafzeh 6 and 9 (Qa 6, Qa 9), Skhul 5 (Sk 5). Upper Palaeolithic modern humans include Cro-Magnon 1 and 3 (CroM 1 CroM 3), Mladeč 1 and 5 (Mla 1, Mla 5), Brno 3, Předmostí 3 and 4 (Pre 3, Pre 4), Abri Pataud (AbP), Cioclovina (Ci), Zhoukoudian Upper Cave 1 and 2 (ZhUC 1, ZhUC 2). The RMH samples are composed of individuals of diverse geographical origins (n=232 in Figure 3a, n=55 in Figure 3b, n=263 in Extended Data Figure 4).

Crown outline analysis *(Extended Data Figure 3a)*

The crown outline analysis of Irhoud 10 and Irhoud 21 left M[1] follows the protocol described in Benazzi *et al.*[39] and Bailey *et al.*[40]. For Irhoud 10, CT images were virtually segmented using a semiautomatic threshold-based approach in Avizo to reconstruct a 3D digital model of the tooth, which was then imported in Rapidform XOR2 (INUS Technology, Inc., Seoul, Korea) to compute the cervical plane. The tooth was aligned with the cervical plane parallel to the xy-plane of the Cartesian coordinate system and rotated around the z-axis with the lingual side parallel to the x-axis. The crown outline corresponds to the silhouette of the oriented crown as seen in occlusal view and projected onto the cervical plane. For Irhoud 21, an occlusal image of the crown was taken with a Nikon D700 digital camera and a Micro-Nikkor 60 mm lens. The tooth was oriented so that the cervical border was perpendicular to the optical axis of the camera lens. The image was imported in Rhino 4.0 Beta CAD environment (Robert McNeel & Associates, Seattle, WA) and aligned to the xy-plane of the Cartesian coordinate system. The crown

outline was digitised manually using the spline function, and then oriented with the lingual side parallel to the x-axis. Both crown outlines[41] were first centered superimposing the centroids of their area according to the M[1] sample created by Bailey *et al.*[40], but integrated with 10 late early and middle Pleistocene *Homo* M[1] specimens (i.e., Arago-31, AT-406, ATD6-11, ATD6-69, ATD6-103, Bilzingsleben-76-530, Petralona, Steinheim, Rabat, Thomas-3). Then, the outlines were represented by 24 pseudolandmarks obtained by equiangularly spaced radial vectors out of the centroid (the first radius is directed buccally and parallel to the y-axis of the Cartesian coordinate system), and scaled to unit centroid size[39,41]. Late early and middle Pleistocene archaic samples include Arago 31 (Ar 31), Atapuerca Gran Dolina 6-11, 6-69, 6-103 (ATD6-11, ATD6-69, ATD6-103), Atapuerca Sima de los Huesos 406 (AT-406), Bilzingsleben-76-530 (Bil76-530), Petralona (Petr), Steinheim (Stein), Rabat (Rab), Thomas 3 (Tho 3). Neanderthal samples include Arcy-sur-Cure 39, Cova Negra, Krapina KDP 1, Krapina KDP 3, Krapina KDP 22, Krapina D101, Krapina D171, Krapina Max C, Krapina Max D, La Ferrassie 8, La Quina H18, Le Fate XIII, Le Moustier 1, Monsempron 1953-1, Obi Rakhmat, Petit Puymoyen, Roc de Marsal, Saint-Césaire 1. EMH include Dar es-Soltan II-NN (DSII-NN), Dar es-Soltan II-H6 (DSII-H6), Qafzeh 10 (Qa 10), Qafzeh 15 (Qa 15), Skhul 1 (Skh 1), Contrebandiers H7 (CT H7). Upper Palaeolithic modern humans include Abri Pataud, Fontéchevade, Gough's Cave (Magdalenian), Grotta del Fossellone, Kostenki 15, Lagar Velho, Laugerie-Basse, La Madeleine, Les Rois 19, La Rois unnumbered, Mladeč 1, Mladeč 2, Peskő Barlang, St. Germain 2, St. Germain B6, St. Germain B7, Sunghir 2, Sunghir 3, Veyrier 1. The RMH samples are composed of individuals of diverse geographical origins (n=80)

Molar and premolar enamel-dentine junction shape analysis *(Extended Data Figure 3b)*

Enamel and dentine tissues of lower second molars and fourth premolars were segmented using the 3D voxel value histogram and its distribution of grey-scale values Skinner *et al.* [42,43]. After the segmentation the EDJ was reconstructed as a triangle-based surface model using Avizo (using unconstrained smoothing). Small EDJ defects were corrected digitally using the "fill holes" module of Geomagic Studio. We then used Avizo to digitise 3D landmarks and curve-semilandmarks on these EDJ surfaces[42,43]. For the molars, anatomical landmarks were placed on the tip of the dentine horn of the

protoconid, metaconid, entoconid, and hypoconid. For the premolars anatomical landmarks were placed on protoconid and metaconid dentine horns. Moreover, we placed a sequence of landmarks along the marginal ridge connecting the dentine horns beginning at the top of the protoconid moving in lingual direction; the points along this ridge curve were then later resampled to the same point count on every specimen using Mathematica. Likewise, we digitised and resampled a curve along the cemento-enamel junction as a closed curve starting and ending below the protoconid horn and the mesio-buccal corner of the cervix. The resampled points along the two ridge curves were subsequently treated as sliding curve semilandmarks and analysed using GMM together with the four anatomical landmarks. *Homo erectus* includes KNM-BK 67, KNM-ER 992 (M_2 and P_4), S1b (M_2 and P_4), S5, S6a. We also included the *Homo habilis*[44] specimen KNM-ER-1802 to establish trait polarity. MP archaic samples include Mauer (Mauer; M_2 and P_4), Balanica BH-1 (Bal). Neanderthal samples include Abri Suard S36, Combe Grenal 29, Combe Grenal IV, Combe Grenal VIII, El Sidron 303, El Sidron 540, El Sidron 755, El Sidron 763a, Krapina 53, Krapina 54, Krapina 55, Krapina 57, Krapina 59, Krapina D1, Krapina D6, Krapina D9, Krapina D35, Krapina D50, Krapina D80, Krapina D86, Krapina D105, Krapina D107, La Quina H9, Le Moustier (M_2 and P_4), Le Regourdou (M_2 and P_4), Scladina (M_2 and P_4), Vindija 11-39. EMH include Dar es-Soltan II H4 (DS II-H4), El Harhoura (El H; M_2 and P_4), Irhoud 11 (Ir 11; M_2 and P_4), Irhoud 3 (Ir 3; M_2 and P_4), Qafzeh 9 (M_2 and P_4), Qafzeh 10, Qafzeh 11 (M_2 and P_4), Qafzeh 15, Contrebandiers (CT; M_2 and P_4). The RMH samples are composed of individuals of diverse geographical origins (M_2 sample n=8; P_4 sample n=8).

Tooth root shape analysis *(Extended Data Figure 3)*

Dental tissues (enamel, dentine and pulp) of the anterior dentition were first segmented semiautomatically using a region growing tool, and when possible using the watershed principle[45]; this segmentation was edited manually to correct for cracks. Each tooth was then virtually divided into crown and root by cutting the 3D models at the cervical plane defined by a least square fit plane between landmarks set at the points of greatest curvature on the labial and lingual sides of the cement-enamel junction. Following Le Cabec *et al.*[46] we analysed dental root shape: using Avizo, a landmark was digitised at the root apex and a sequence of 3D landmark coordinates was recorded along the cement-

enamel junction. Using Mathematica, this curve was then resampled to 50 equidistant curve-semilandmarks. The shape of the root surface, delimited by the cervical semilandmarks and the apical landmark, was quantified using 499 surface-semilandmarks[46]: a mesh of 499 landmarks was digitised manually on a template specimen, then warped to each specimen using a thin-plate spline interpolation and lofted onto the segmented root surface by projecting to closest surface vertex. These landmarks and semilandmarks were then analysed using GMM. *Homo erectus* is represented by KNM-WT 15000 (WT 15000). The Neanderthal sample includes Krapina 53, 54, 55, 58, 59 (Krp53, Krp 54, Krp 55, Krp 58, Krp 59), Saint-Césaire 1 (SC), Abri-Bourgeois-Delaunay 1 (BD1), and Kebara 2 and 28 (Keb 2, KMH 28). EMH include Contrebandiers (CT), Dar es-Soltan II-H4 (DSII-H4) and El Haroura (El H). Upper Palaeolithic and Mesolithic modern samples include individuals from Oberkassel (Ob), Nahal-Oren (NO 8, NO 14), Hayonim (Ha 8, Ha 19, Ha 20), Kebara (KebA5) and Combe-Capelle (CC). The RMH sample includes individuals of diverse geographical origins (n=47)

Statistical analysis

3D landmark and semilandmark data were analysed using GMM functions in Mathematica[34,47]. Curves and surfaces were quantified using sliding semilandmarks based on minimizing the thin-plate spline bending energy[32] between each specimen and the sample mean shape[33, 34]. Missing landmarks or semilandmarks were estimated using a thin-plate spline interpolation based on the sample mean shape during the sliding process[48]. After sliding, all landmarks and semilandmarks were converted to shape variables using generalised least squares Procrustes superimposition[49]; these data were then analysed using principal component analysis (PCA), and between group PCA[50]. For the M^1 crown outlines analysis, the shape variables of the outlines were projected into the shape-space obtained from a principal component analysis (PCA) of the M^1 comparative sample. The data were processed and analysed through software routines written in R[51].

Mandibular metric data *(Extended Data Table 2 and Extended Data Figure 1c)*

Linear measurements were taken on 3D surface models generated from microCT data in Avizo. They were complemented by measurements of the original specimens taken by E. Trinkaus (Extended Data Fig. 1c) and by comparative data taken from the literature[52-99]. The African and European MP archaic sample includes KNM-BK 67, KNM-BK 8518, Sidi

Abderrahmane 2, Thomas Quarry I, Thomas Quarry Gh 10717, Tighenif 1, 2, 3, Arago I, XIII, Mauer, Montmaurin 1, Sima de los Huesos XIX, XXI, XXVIII, AT 1, AT 75, AT 300, AT 605, AT 607. The Asian Neanderthals include Amud 1, Chagyrskaya 6, Kebara 2, Shanidar 1, 2 and 4 and Tabun C1. The European Neandertals include Arcy II, Banyoles, El Sidrón 1, 2 and 3, Guattari 2 and 3, Hortus 4, Krapina 57, 58 and 59, Suard S 36, Bourgeois Delaunay 1, La Ferrassie 1, La Quina 5, La Naulette 1, Le Regourdou 1, Saint Césaire, Sima de las Palomas 1, 6, 23, 59, Spy 1 and 3, Subalyuk 1, Vindija 206, 226, 231, 250, 11.39, 11.40, 11.45, Weimar-Ehringsdorf F1009 and Zafarraya. The EMH include Dar es-Soltan II H5, El Harhoura 1, Dire Dawa, Klasies River: KRM 13400, 14695, 16424 , 21776 and 41815, Qafzeh 9, 26 and 27, Skhul IV, Skhul V, Tabun C2 and Témara 1. The Upper Palaeolithic and Epipalaeolithic sample includes individuals from Abri Pataud 1, Arene Candide 2 and 18, Asselar, Barma del Caviglione, Chancelade, Cro Magnon 1 and 3, Dar es-Soltan II H2 and H3, Dolni Věstonice 3, 13, 14, 15, 16, El Mirón, Grotte des Enfants 4, Hayonim 8, 17, 19, 20, 25, 27, 29 and 29a, Isturitz and 115, Le Roc 1 and 2, Minat 1, Moh Khiew, Muierii 1, Nahal Oren 6, 8, 14 and 18, Nazlet Khater 2, Oase 1, Oberkassel 1 and 2, Ohalo II 1 and 2, Pavlov 1, Předmostí 3 and 21, Sunghir 1 and 6, Villabruna 1 and Zhoukoudian Upper Cave 101, 104 and 108.

Dental metric and non-metric data *(Extended Data Tables 3, 4 and 5)*

Crown metric and non-metric data were collected from casts or originals with a few exceptions taken from the literature. The latter include: Mumba XII[100]; Eyasi[101]; Kapthurin[102]; Olduvai[103]; Sima de los Huesos[103]; some Sangiran metric data[104]. Root metric data were taken on 3D models generated from micro-computed tomographic data[105, 106]. Crown measurements were taken using Mitituyo digital calipers. Non-metric trait expressions were scored using the Arizona State University Dental Anthropology System[107] where applicable (Lower dentition: P_4 lingual cusps, Cusp 6, Cusp 7, M_2 groove pattern, protostylid; for Upper dentition: shoveling, tuberculum dentale, canine distal accessory ridge, Cusp 5, Carabelli's trait, parastyle, metacone and hypocone reduction), and Bailey[108] for all others. RMH include individuals from South, West and East Africa, Western and Central Europe, Northeast Asia, West Asia, India, Australia, New Guinea and Andaman Islands. For root metrics the sample composition is in Table 1 from Le Cabec *et al.*[106]. *H. erectus* includes individuals from Zhoukoudian, Sangiran, West Turkana, East

Rudolf, Olduvai and Dmanisi. MP African archaics (MPAf) include individuals from Thomas Quarries, Salé, Florisbad, Rabat, Hoedijiespunt, Cave of Hearths, Olduvai, Kapthurin, Mumba, Eyasi, Broken Hill and Sidi Abderrahmane. MP European archaics (MPE) include individuals from Mauer, Arago, Sima de los Huesos, Pontnewydd, Fontana Ranuccio. Neanderthal samples include individuals from Amud, Arcy sur Cure, Cova Negra, Grotta Guattari, Hortus, Kalamakia, Krapina, Kebara, Kulna, La Quina, La Fate, La Ferrassie, Le Moustier, Melpignano, Monte Fenera, Monsempron, Montmaurin, Feldhofer, Obi-Rakhmat, Ochoz, Pech-de-l'Azé, Petit Puymoyen, Regourdou, Roc-de-Marsal, Spy, Saint-Césaire, Subalyuk, Tabun and Vindija. EMH include individuals from Die Kelders, Equus Cave, Klasies River Mouth, Sea Harvest, Haua Fteah, Dar es-Soltan, Contrebandiers, El Harhoura, Qafzeh, and Skhul.

31. Wollny, G. *et al.* MIA - A free and open source software for gray scale medical image analysis. *Source Code for Biology and Medicine* **8**, 1-20, doi:10.1186/1751-0473-8-20 (2013)
32. Bookstein, F. L. Landmark methods for forms without landmarks: morphometrics of group differences in outline shape. *Medical Image Analysis* **1**, 225-243 (1997)
33. Gunz, P., Mitteroecker, P. & Bookstein, F. L. Semilandmarks in three dimensions. in *Modern Morphometrics in Physical Anthropology.* (ed D.E. Slice) 73-98 (Kluwer Academic/Plenum Publishers, 2005)
34. Gunz, P. & Mitteroecker, P. Semilandmarks: a method for quantifying curves and surfaces. *Hystrix, the Intalian Journal of Mammalogy* **24**, 103-109, doi:doi:10.4404/hystrix-24.1-6292 (2013)
35. Wiley, D. F. *et al.* in *16th IEEE Visualization Conference (VIS 2005)* **55**, 431-438 (American Journal of Physical Anthropology, Minneapolis, MN, USA, 2005)
36. Freidline, S. E., Gunz, P., Harvati, K. & Hublin, J.-J. Middle Pleistocene human facial morphology in an evolutionary and developmental context. *Journal of Human Evolution* **63**, 723-740, doi:10.1016/j.jhevol.2012.08.002 (2012)
37. Neubauer, S., Gunz, P. & Hublin, J.-J. The pattern of endocranial ontogenetic shape changes in humans. *Journal of Anatomy* **215**, 240-255 (2009)
38. Harvati, K., Gunz, P. & Grigorescu, D. Cioclovina (Romania): affinities of an early modern European. *Journal of Human Evolution* **53**, 732-746, doi:10.1016/j.jhevol.2007.09.009 (2007)
39. Benazzi, S. *et al.* Early dispersal of modern humans in Europe and implications for Neanderthal behaviour. *Nature* **479**, 525-528, (2011)
40. Bailey, S. E., Benazzi, S. & Hublin, J.-J. Allometry, merism, and tooth shape of the upper deciduous M2 and permanent M1. *American Journal of Physical Anthropology* **154**, 104-114, doi:10.1002/ajpa.22477 (2014)
41. Benazzi, S. *et al.* Cervical and crown outline analysis of worn Neanderthal and modern human lower second deciduous molars. *American Journal of Physical Anthropology* **149**, 537-546, doi:10.1002/ajpa.22155 (2012)

42. Skinner, M. M., Gunz, P., Wood, B. A. & Hublin, J.-J. Enamel-dentine junction (EDJ) morphology distinguishes the lower molars of Australopithecus africanus and Paranthropus robustus. *Journal of Human Evolution* **55**, 979-988 (2008)

43. Skinner, M. M., Gunz, P., Wood, B. A., Boesch, C. & Hublin, J. J. Discrimination of extant Pan species and subspecies using the enamel-dentine junction morphology of lower molars. *American Journal Of Physical Anthropology* **140**, 234-243 (2009)

44. Spoor, F., Gunz, P., Neubauer, S., Stelzer, S., Scott, N., Kwekason, A., and Dean. C., 2015. Reconstructed homo habilis type OH 7 suggests deep-rooted species diversity in early homo. *Nature* 519 (7541): 83-6 (2015)

45. Beucher, S. & Lantuéjoul, C. in *International workshop on image processing: real-time edge and motion detection*, 2.1-2.12 (Rennes, France, 1979)

46. Le Cabec, A., Gunz, P., Kupczik, K., Braga, J. & Hublin, J.-J. Anterior tooth root morphology and size in Neanderthals: Taxonomic and functional implications. *Journal of Human Evolution* **64**, 169-193, doi:http://dx.doi.org/10.1016/j.jhevol.2012.08.011 (2013)

47. Mitteroecker, P. & Gunz, P. Advances in Geometric morphometrics. *Evolutionary Biology* **36**, 235-247 (2009)

48. Gunz, P., Mitteroecker, P., Neubauer, S., Weber, G. W. & Bookstein, F. L. Principles for the virtual reconstruction of hominin crania. *Journal of Human Evolution* **57**, 48-62 (2009)

49. Rohlf, F. J. & Slice, D. Extensions of the Procrustes Method for the Optimal Superimposition of Landmarks. *Systematic Zoology* **39**, 40-59, doi:10.2307/2992207 (1990)

50. Mitteroecker, P. & Bookstein, F. Linear Discrimination, Ordination, and the Visualization of Selection Gradients in Modern Morphometrics. *Evolutionary Biology* **38**, 100-114, doi:10.1007/s11692-011-9109-8 (2011)

51. R Development Core Team. R: a language and environment for statistical computing. R Foundation for Statistical Computing, Vienna, Austria. http://www.r-project.org (2012)

52. Arambourg, C., Biberson, P. The fossil human remains from the Paleolithic site of Sidi Abderrahman (Morocco). *Am. J. Phys. Anthropol.* **14**, 467-489 (1956)

53. Sausse, F. La mandibule atlanthropienne de la carrière Thomas I (Casablanca). *Anthropologie* **79**, 81-112 (1975)

54. Deacon, H. J. Comparative studies of Late Pleistocene human remains from Klasies River Mouth, South Africa. *J. Hum. Evol.* 20, 131-156 (1991)

55. Stewart, Th. D. The skull of Shanidar II. In: *Annual Report of the Smithsonian Institution*, 521-533 (1962)

56. Tillier, A.-M. La mandibule et les dents. In: *Le Squelette moustérien de Kébara 2*, 97-11 (1991)

57. Stewart, T. D. The Neanderthal Skeletal Remains from Shanidar Cave, Iraq: A Summary of Findings to Date. Proceedings of the American Philosophical Society **121**, 121-165 (1977)

58. Trinkaus, E., *The Shanidar Neanderthals.* Academic Press, New York. (1983)

59. Leroi-Gourhan, A. *Étude des restes humains fossiles provenant des Grottes d'Arcy-sur-Cure.* Masson et Cie, Paris. (1958)

60. Daura, J., Sanz, M., Subirá, M. E., Quam, R., Fullola, J. M., & Arsuaga, J. L., A Neandertal mandible from the Cova del Gegant (Sitges, Barcelona, Spain). *J. Hum. Evol.*, **49**, 56-70 (2005)

61. Topinard, P., Les caracteres simiens de la machoire de la Naulette. *Revue d'anthropologie* **15**, 385-431 (1886)

62. Blake, C. C. On a Human Jaw from the Cave of La Naulette, near Dinant,Belgium. *Anthropological Review* **5**, 294-303 (1867)

63. Leguebe, A., Toussaint, M., La mandibule et les cubitus de la Naulette: morphologie et morphométrie. *Editions du Centre national de la recherche scientifique* **15,** (1988)

64. Heim, J. L. Les hommes fossiles de La Ferrassie (Dordogne) et le probleme de la definition des Neandertaliens classiques. III. *Squelette céphalique. L'Anthropologie* **78**, 321-378 (1974)

65. Lumley, M.-A. *Les Néandertaliens de la grotte de l'Hortus. Etudes Quaternaires 1*, 375-385, (1972)

66. Condemi, S., Mounier, A., Giunti, P., Lari, M., Caramelli, D., & Longo, L., Possible Interbreeding in Late Italian Neanderthals? New Data from the Mezzena Jaw (Monti Lessini, Verona, Italy). *PloS one,* **8**, e59781, (2013)

67. Corrain, C. Resti scheletrici umani del 'Riparo Mezzena'. *Memorie del Museo civico di Storia naturale di Verona* **16**, 97-101 (1968)

68. Walker, M. J., Lombardi, V. A., Zapata, J., Trinkaus, E. Neandertal mandibles from the Sima de las Palomas del Cabezo Gordo, Murcia, southeastern Spain. *Am. J. of Phys. Anthropol*. **142**, 261-272 (2010)

69. Martin, H. Machoire humaine moustérienne trouvée dans la station de La Quina. *L'homme préhistorique* **13**, 3-21 (1926)

70. Martin, H. Position stratigraphique des Ossements humains recueillis dans le Moustérien de La Quina de 1908 à 1912. *Bulletin de la Société préhistorique de France* **9**, 700-709 (1912)

71. Martin, H. *L'Homme fossile de la Quina*. Libraire Octave Doin, Paris. (1923)

72. Pap, I., Tillier, A. M., Arensburg, B., Chech, M. The Subalyuk Neanderthal remains (Hungary): a re-examination. *Annales Historico Naturales-Musei Nationalis Hungarici* 88, 233–270 (1996)

73. Sanchez, F., Comparative biometrical study of the Mousterian mandible from Cueva del Boquete de Zafarraya (Málaga, Spain). *Human Evolution* **14**, 125-138 (1999)

74. Vlček, E. Fossile Menschenfunde von Weimar-Ehringsdorf. *Weimarer Monographien zur Ur- und Frühgeschichte,* **30**, (1993)

75. Condemi, S. *Les néandertaliens de La Chaise: abri Bourgeois-Delaunay. Comité des travaux historiques et scientifiques-CTHS* (2001)

76. Bar-Yosef, O., & Vandermeersch, B. (Eds.). *Le squelette moustérien de Kébara 2. Editions du Centre national de la recherche scientifique.* (1991)

77. Arambourg, C., & Hoffstetter, R. *Le gisement de Ternifine* (Vol. 1). Masson, Paris. (1963)

78. Hooton, E.A., Hencken, H.O., Snow, Ch. E. *The ancient Palestinian: Skhūl V reconstruction.* American school of prehistoric research*. **17**, 5-10 (1953)

79. Rightmire, G. Ph., Deacon, H. J. Comparative studies of Late Pleistocene human remains from Klasies River Mouth, South Africa. *J. Hum. Evol.* **20**, 131-156 (1991)

80. Sollas, W. J. The Chancelade Skull. *The Journal of the Royal Anthropological Institute of Great Britain and Ireland* **57**, 89-122 (1927)

81. Martin, H. Caractères des squelettes humains quaternaires de la vallée du Roc (Charente).Race de Chancelade. *Bulletins et memoires de la Société d'anthropologie de Paris.* **8**, 103-129 (1927)

82. Vercellotti, G., Alciati, G., Richards, M. P., & Formicola, V. The Late Upper Paleolithic skeleton Villabruna 1 (Italy): a source of data on biology and behavior of a 14.000 year-old hunter. *J Anthropol Sci*, **86**, 143-163 (2008)

83. Formicola, V. Una mandibola umana dal deposito dell'Epigravettiano finale delle Arene Candite (scavi 197O). *Rivista di antropologia* **64**, 271-278 (1986)

84. Odano, A. M., Riquet, R. Le gisement préhistorique de Dar-es-Soltane 2. Champ de tir de El Menzeh à Rabat (Maroc). Note préliminaire. 2-Étude anthropologique des restes post-atériens. *Bull. d'Archéologie Marocaine* **11**, 25-63 (1978)

85. Debénath, A. Nouveaux restes humains atériens du Maroc. *CR Acad. Sci. Paris* **290**, 851-852 (1980)

86. Crognier, E., Dupouy-Madre, M. Les Natoufiens du Nahal Oren (Ouadi Fallah) Etude anthropologique. *Paléorient* **2**, 103-121 (1974)

87. Henke, W. Vergleichend-morphologische Kennzeichnung der Jungpaläolithiker von Oberkassel bei Bonn. *Zeitschrift für Morphologie und Anthropologie* **75**, 27-44 (1984)

88. Hershkovitz, I. Ohalo II H2: a 19,000-year-old skeleton from a water-logged site at the Sea of Galilee, Israel. *Am. J. Phys. Anthropol.* **96**, 215-234 (1995)

89. Soficaru, A., Dobos, A., Trinkaus, E. Early modern humans from the Pestera Muierii, Baia de Fier, Romania. *Proceedings of the National Academy of Sciences of the United States of America* **103**, 17196-17201 (2006)

90. Crevecoeur, I. *Etude anthropologique des restes humains de Nazlet Khater (Paléolithique Superieur, Egypte).* PhD Thesis, Université Sciences et Technologies - Bordeaux I. (2006)

91. Thoma, A. Morphology and affinities of the Nazlet Khater man. *J. Hum. Evol.* **13**, 287-296. (1984)

92. Anderson, J. E. Late Paleolithic skeletal remains from Nubia. *The prehistory of Nubia vol. 2* (ed. Wendorf, F.) 996-1040 (Dallas, Fort Burgwin Research Center & Southern Methodist University Press,1968)

93. Crevecoeur, I. From the Nile to the Danube: a comparison of the Nazlet Khater 2 and Oase 1 early modern human mandibles. *Anthropologie (Brno)* **42**, 203-213 (2004)

94. Trinkaus, E. et.al. An early modern human from the Peştera cu Oase, Romania. *Proceedings of the National Academy of Sciences*, **100**, 11231-11236 (2003)

95. Trinkaus, E., Svoboda, J. *Early modern human evolution in Central Europe: the people of Dolní Věstonice and Pavlov.* The Dolni Vestonice Studies vol. 12. (New York, Oxford University Press, 2006)

96. Sládek, V., Trinkaus, E., Hillson, S. W., & Holliday, T. W. *The people of the Pavlovian. Skeletal catalogue and osteometrics of the Gravettian fossil hominids from Dolni Vestonice and Pavlov*. Dolni Vestonice Studie, Svazek 5, 1-244. (2000)

97.   Drozdová, E. The evaluation of a rediscovered fragment of human lower jaw, No 21 from Předmostí u Přerova. *Archeologické rozhledy* **53**, 452-460 (2001)

98.   Dutour, O. Palimpseste paléoanthropologique sur l'«Homme fossile d'Asselar» (Sahara). Travaux du Laboratoire d'Anthropologie et de Préhistoire des Pays de la Méditerranée Occidentale 1, 73–83 (1992).

99.   Gambier, D. Vestiges humains du gisement d'Isturitz (Pyrénées-Atlantiques): étude anthropologique et analyse des traces d'action humaine intentionelle. *Antiquités nationales* **22-23,** 9-26 (1990)

100.   Bräuer, G. & Mehlman, M. J. Hominid molars from a Middle Stone Age level at   Mumba Rock Shelter, Tanzania. *Am. J. Phys. Anthropol.* **75**, 69-76 (1988).

101.   Protsch, R. R. R. *Di Archäologischen und Anthropologischen Ergebnisse der Kohl-Larsen-Expeditionen in Nord-Tanzania 1933-1939*. (Institut für Urgeschichte der Universität Tübingen, 1981).

102.   Wood, B. A. & van Noten, F. L. Preliminary observations on the BK 8518 mandible from Baringo, Kenya. *Am. J. Phys. Anthropol.* **69**, 117-127, doi:10.1002/ajpa.1330690113 (1986).

103.   Rightmire, G. P. Middle Pleistocene hominids from Olduvai Gorge, Northern Tanzania. *Am. J. Phys. Anthropol.* **53**, 225-241, doi:10.1002/ajpa.1330530207 (1980).

104.   Bermúdez de Castro, J. M. Dental remains from Atapuerca (Spain) I. Metrics. *Journal of Human Evolution* **15**, 265-287 (1986).

105.   Grine, F. E. & Franzen, J. L. Fossil hominid teeth from the Sangiran Dome (Java, Indonesia). *Courier Forschungsinstitut Senckenberg* **171**, 75-103 (1994).

106.   Le Cabec, A., Gunz, P., Kupczik, K., Braga, J. & Hublin, J.-J. Anterior Tooth Root Morphology and Size in Neanderthals: Taxonomic and Functional Implications. *J. Hum. Evol.* **64**, 169-193, doi:10.1016/j.jhevol. 2012.08.011 (2013).

107.   Turner CG, II, Nichol CR, and Scott GR. 1991. Scoring procedures for key morphological traits of the permanent dentition: The Arizona State University Dental Anthropology System. In: Kelley M, and Larsen C, editors. Advances in Dental Anthropology. New York: Wiley Liss. p 13-31.

108.   Bailey SE. 2002. Neandertal Dental Morphology: Implications for modern human origins [Ph.D. Dissertation]. Tempe: Arizona State University. 238 p.

Figure captions

Figure 1 | Facial reconstruction of Irhoud 10, frontal **(a)** and basal **(b)** views. This Procrustes superimposition of Irhoud 10 (beige) and Irhoud 1 (light blue) represents one possible alignment of the facial bones of Irhoud 10. Multiple alternative reconstructions (*n*=9) were included in the statistical shape analysis of the face (see Methods and Figure 3). The maxilla, zygomatic bone and supra-orbital area on Irhoud 10 are more robust than on Irhoud 1. Scale is 20 mm.

Figure 2 | Irhoud 11 mandible (lateral and cranial views). See Methods for the reconstruction. The bi-condylar breadth of the Irhoud 11 mandible exactly fits the width of the corresponding areas on the Irhoud 2 skull. Scale is 20 mm.

Figure 3 | Comparative shape analysis. **a,** PCA of the facial shape. EMH and RMH are well separated from Neanderthals and archaic MP hominins. Irhoud 1 and all nine alternative reconstructions of Irhoud 10 (pink stars and pink 99% confidence ellipse, see Methods) fall within the RMH variation. **b,** PCA of endocranial shape. RMH (blue), Neanderthals (red) and *Homo erectus* (green) are separated. Archaic MP Hominins (orange) plot with Neanderthals. Irhoud 1 and 2 (pink stars) and some EMH (black) fall outside the RMH variation. Shape differences are visualized in Extended Data Figure 5a. Sample compositions and abbreviations are in Methods.
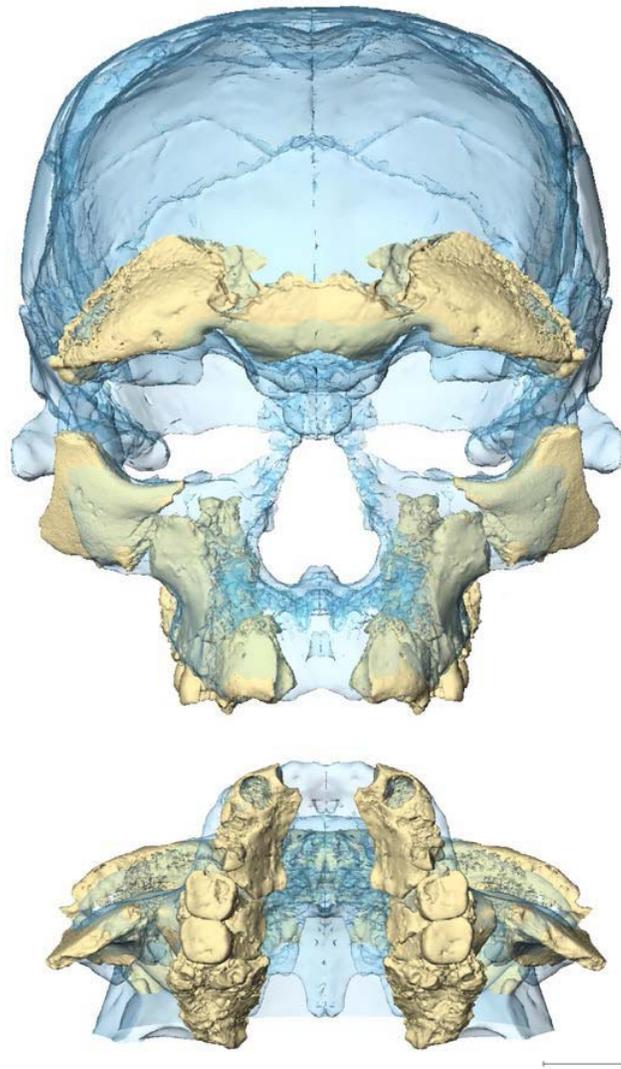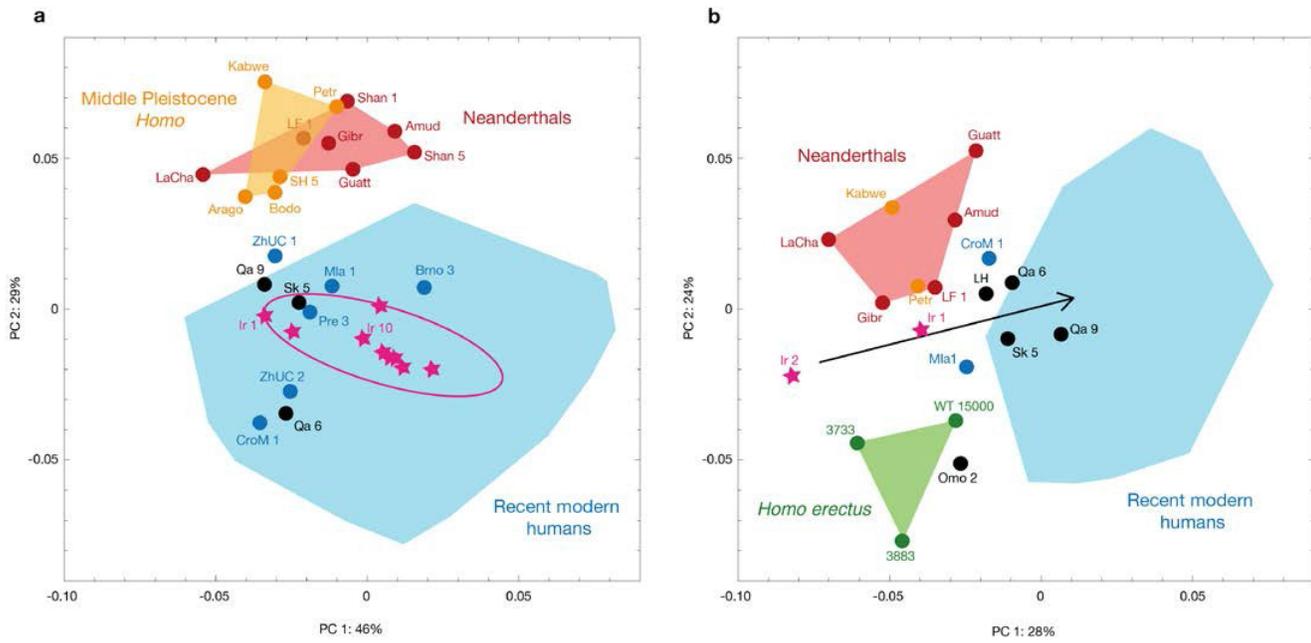
Figure 1

Figure 2

Figure 3

Extended Data Figure Captions

Extended Data Table 1| List of hominin specimens. Starting with the 2004 excavation, specimens were given ID numbers from the project catalogue. Layer 18 of the excavation by de Bayle des Hermens and Tixier[6] corresponds to Layer 7 of the 2004-2011 excavation.

Extended Data Table 2| Measurements of the Irhoud 11 mandible after reconstruction. They are compared to those of five groups of fossil hominins. Values in mm. $\bar{x}$ = mean value, σ = standard deviation, n= sample size. The value with "?" is an estimate. Data sources and sample compositions are in Methods.

Extended Data Table 3| Dental measurements (upper dentition) BL = Bucco-lingual width, MD = Mesio-distal length. Values in mm. $\bar{x}$ = mean value; minimum and maximum values are between square brackets; σ = standard deviation; n= sample size. Values in parentheses represent uncorrected measurements on worn or cracked teeth. Data sources and sample compositions are in Methods.

Extended Data Table 4| Dental measurements (lower dentition). BL = Bucco-lingual width, MD = Mesio-distal length, RL = Root Length. All values in mm. $\bar{x}$ = mean value; minimum and maximum values are between square brackets; σ = standard deviation; n= size of the sample. Values in parentheses represent uncorrected measurements on worn or cracked teeth. Data sources and sample compositions are in Methods.

Extended Data Table 5| Morphological dental trait comparison

Numbers given are trait frequencies score at the enamel surface. Sample sizes are in brackets. Data sources and sample compositions are in Methods.

Extended Data Figure 1 | Mandibular morphology. a, Symphyseal section of Irhoud 11 mandible showing the mental angle. **b,** Mental area of Irhoud 11 before virtual reconstruction (top) and Irhoud 3 (bottom). Both figures are surface models generated from micro CT data. **c,** Bivariate plot of mandibular corpus breadth versus height at the mental foramen. Values in

mm. Irhoud 11 plots with EMH and displays one of the largest corpus height among middle to late Pleistocene hominins. "n" indicates sample size. Data sources and sample compositions are in Methods.

Extended Data Figure 2 | **a, shape–space PCA plot of late early and middle Pleistocene archaic *Homo*, Neanderthals and RMH M^1 crown outlines**. The deformed mean crown outlines in the four directions of the PCs are drawn at the extremity of each axis. Sample compositions and abbreviations are in Methods. **b, Enamel-dentine junction (EDJ) morphology of the M$_2$ and P$_4$.** At top left a PCA analysis of EDJ shape of the M$_2$ places Irhoud 11 intermediate between *H. erectus* and RMH (along with other north Africa fossil humans) and distinct from Neanderthals. Surface models illustrate EDJ shape changes along PC1 (bottom left) and PC2 (top right); the former separating *H. erectus* from RMH, Neanderthals and North African EMH and the latter separating Neanderthals from RMH and north African EMH. At bottom right a PCA analysis of EDJ shape of the P$_4$ groups Irhoud 11 with modern and fossil humans.

Extended Data Figure 3 | Shape analysis of I$_2$ roots. A between-group PCA shows a complete separation between Neanderthals and a worldwide sample of recent modern humans based on subtle shape differences. Irhoud 11 (magenta) plots at the fringes of RMH, close to the EMH from Temara. Colour-coded Procrustes group mean shapes are plotted in the same orientation as the I$_2$ root surface of Irhoud 11. Although Irhoud 11 is more similar, overall, to Neanderthals in terms of root size, its root shape is clearly modern. The *Homo erectus s.l.* specimen KNM-WT 15000 and hypothetical EMH Tabun C2 have incisor root shapes similar to Neanderthals, suggesting that roots that are labially more convex than in RMH represent a conserved primitive condition with limited taxonomical value. Sample compositions and abbreviations are in Methods.

Extended Data Figure 4 | Shape analysis of external vault. a, Principal component (PC) scores 1 vs. 2 of external braincase shape in *Homo erectus*, MP archaic *Homo*, a geographically

diverse RMH and Neanderthals. Results are consistent with the analysis of endocranial shape (Figure 3a). However, several EMH and Upper Palaeolithic specimens fall outside the RMH variation. This is likely due to the projecting supraorbital tori in these specimens. **b**, Shape changes associated with PC 1 (two standard deviations in either direction) shown as thin-plate spline deformation grids in lateral and oblique view. PC 1 captures a contrast between elongated braincases with projecting supraorbital tori (low scores in black), and a more globular braincase with gracile supraorbital tori (high scores in red). Sample compositions and abbreviations are in Methods.

Extended Data Figure 5 | Facial and endocranial shape differences among *Homo* groups.
Visualizations of GMM shape analyses in Figure 3. **a**, Average endocranial shape differences *Homo erectus*, recent *Homo sapiens*, and Neanderthals. Thin-plate spline (TPS) grids are exaggerated. **b**, Visualisation of shape changes along principal component (PC) 1 in Figure 3b in frontal, lateral and superior view; two standard deviations in either direction from the mean shape (grey, negative; black: positive). **c**, Shape changes along PC 2. All recent and fossil modern humans (low scores along PC 2) share smaller, orthognathic faces, that differ from the larger, robust and prognathic faces of the middle Pleistocene humans and Neanderthals (high scores along PC 1). Arrow length is colour coded (short: blue; long: red). As these visualisations are affected by the Procrustes superimposition, we also show TPS-grids in the maxilla and the supraorbital area. The arrow points to the plane of the maxillary TPS (red) in the template configuration.

Specimens	Item ID	Anatomical part	Year	Stratigraphic position
Irhoud 1	No ID	Cranium	1961	Lower deposits[4]
Irhoud 2	No ID	Cranium	1962	Lower deposits[4]
Irhoud 3	No ID	Mandible (juvenile)	1968	Lower deposits[5]
Irhoud 4	No ID	Humerus (juvenile)	1969	Layer 18 of Tixier[6]
Irhoud 5	No ID	Coxal (juvenile)	1969	Layer 18 of de Bayle des Hermens & Tixier[7]
Irhoud 6	No ID	Mandible fragment	1961-69	Identified among faunal remains
Irhoud 7	4766	Lower right P3	2004	Initial cleaning
Irhoud 8	4767	Distal part of left lower molar	2004	Initial cleaning
Irhoud 9	1653	Lower Molar (M1 or M2)	2006	Layer 4
Irhoud 10	1678, 1679, 1680, 2178, 2259	Cranium	2007	Layer 7
Irhoud 11	4765 + 3752	Mandible	2007	Layer 7
Irhoud 12	2196	Lower incisor	2007	Layer 7
Irhoud 13	2252	Left proximal Femur	2007	Layer 7
Irhoud 14	2381, 2383	Rib	2009	Layer 7
Irhoud 15	2401	Rib	2009	Layer 7
Irhoud 16	2561, 2565	Humerus (juvenile)	2009	Layer 7
Irhoud 17	2670	Right proximal Femur	2009	Layer 7
Irhoud 18	2838	Lumbar vertebra	2007	Initial cleaning
Irhoud 19	3747, 3748, 3749	Fibula	2009	Layer 7
Irhoud 20	3751	Cervical vertebra	2009	Initial cleaning
Irhoud 21	4200	Maxilla	2011	Layer A
Irhoud 22	4502, 4503	M2 and M3 sup	2011	Layer A

Extended Data Table 1

Measurement	Irhoud 11	African and European archaic MP	Asian Neanderthals	European Neanderthals	Early *modern* humans	Upper Palaeolithic MH
Symphyseal Height	45	$\bar{x}$ = 31.53 σ = 3.7 n = 13	$\bar{x}$ = 36.1 σ = 3.36 n = 6	$\bar{x}$ = 33.98 σ = 4.64 n = 21	$\bar{x}$ = 36.36 σ = 6.03 n = 8	$\bar{x}$ = 31.87 σ = 2.82 n = 38
Corpus Height at Mental Foramen	38.4	$\bar{x}$ = 30.69 σ =4.2 n = 19	$\bar{x}$ = 33.9 σ =3.51 n = 7	$\bar{x}$ = 31.22 σ = 3.43 n = 33	$\bar{x}$ = 34.23 σ = 4.57 n = 13	$\bar{x}$ = 30.89 σ = 3.11 n = 47
Corpus Breadth at Mental Foramen	15.4	$\bar{x}$= 17.22 σ = 1.98 n = 19	$\bar{x}$ = 17.16 σ = 1.89 n = 7	$\bar{x}$ = 15.56 σ = 1.71 n = 33	$\bar{x}$ = 16.04 σ = 1.75 n = 13	$\bar{x}$ = 12.67 σ = 1.55 n = 48
Corpus Height at M_1	36	$\bar{x}$ = 31.15 σ = 4.59 n = 15	$\bar{x}$ =31.65 σ = 3.17 n = 4	$\bar{x}$ = 30.82 σ = 3.36 n = 22	$\bar{x}$ = 32.81 σ = 5.64 n = 10	$\bar{x}$ = 29.51 σ = 2.19 n = 29
Corpus Breadth at M_1	17.7	$\bar{x}$ = 17.57 σ = 2.4 n = 15	$\bar{x}$ = 17.54 σ = 2.67 n = 5	$\bar{x}$ = 16.7 σ = 1.75 n = 22	$\bar{x}$ = 17.11 σ = 2.57 n = 11	$\bar{x}$ = 14.25 σ = 1.57 n = 26
Corpus Height at M_1/M_2	34	$\bar{x}$ = 30.82 σ = 4.21 n = 15	$\bar{x}$ = 32.40 σ = 1.65 n = 3	$\bar{x}$ = 29.64 σ = 3.21 n = 23	$\bar{x}$ = 32.88 σ = 4.26 n = 8	$\bar{x}$ = 28.64 σ = 2.3 n = 33
Corpus Breadth at M_1/M_2	19.3	$\bar{x}$ = 18.03 σ = 2.98 n = 15	$\bar{x}$ = 17.57 σ = 2.25 n = 3	$\bar{x}$ = 16.35 σ = 1.56 n = 22	$\bar{x}$ = 17.56 σ = 2.43 n = 8	$\bar{x}$ = 14.73 σ = 1.92 n = 34
Corpus Height at M_2	31,5	$\bar{x}$ = 30.42 σ =3.97 n = 20	$\bar{x}$ = 31.75 σ = 3.82 n = 6	$\bar{x}$ = 30.10 σ = 3.4 n = 26	$\bar{x}$ = 32.41 σ = 5.22 n = 8	$\bar{x}$ = 27.04 σ = 2.58 n = 34
Corpus Breath at M_2	22.7	$\bar{x}$ = 18.45 σ = 2.45 n =20	$\bar{x}$ = 17.6 σ = 1.54 n = 7	$\bar{x}$ = 16.03 σ = 1.78 n = 25	$\bar{x}$ = 18.48 σ = 2.93 n = 8	$\bar{x}$ = 15.02 σ = 1.89 n = 36
Length of the Dental Arcade	66.5	$\bar{x}$ = 58.19 σ = 5.46 n = 11	$\bar{x}$ = 54.78 σ = 2.78 n = 4	$\bar{x}$ = 55.23 σ = 2.49 n = 10	$\bar{x}$ = 57.25 σ = 6.22 n = 4	$\bar{x}$ = 51.78 σ = 3.33 n = 26
Bigonial Breadth	144 ?	$\bar{x}$= 96.93 σ = 11.84 n = 6	$\bar{x}$ = 102.13 σ = 6.22 n = 4	$\bar{x}$ = 92.57 σ = 11.62 n = 6	$\bar{x}$ = 93.75 σ = 13.93 n = 4	$\bar{x}$ = 98.59 σ = 9.67 n = 29
Bicanine Breadth	38.5	$\bar{x}$ = 35.54 σ = 3.79 n = 11	$\bar{x}$ = 36.48 σ = 1.63 n = 6	$\bar{x}$ = 36.62 σ = 2.45 n = 14	$\bar{x}$ = 38.0 σ = 2.00 n = 5	$\bar{x}$ = 32.64 σ = 2.38 n = 28
Bi-M_2 Breadth	66.6	$\bar{x}$ = 66.13 σ = 5.81 n = 11	$\bar{x}$ = 72.1 σ = 1.48 n = 4	$\bar{x}$ = 69.86 σ = 3.23 n = 11	$\bar{x}$ = 68.46 σ = 3.54 n = 5	$\bar{x}$ = 61.75 σ = 3.88 n = 26
Bi-M_3 Breadth	70.9	$\bar{x}$ = 70.24 σ = 6.22 n = 11	$\bar{x}$ = 74.86 σ = 2.78 n = 5	$\bar{x}$ = 71.9 σ = 3.29 n = 11	$\bar{x}$ = 72.03 σ = 4.16 n = 4	$\bar{x}$ = 66.62 σ = 4.07 n = 26

Extended Data Table 2

		Irhoud 10	Irhoud 21	Irhoud 22	*H. erectus*	MPE	MPAf	Neanderthals	EMH	RMH
C′	BL	--	9.8	--	x̄ = 10.3 [9.7-11.9] σ = 0.7 n=12	x̄ =9.8 [8.8-10.7] σ =0.7 n=6	x̄ = 9.7 [8.9-10.5] σ =1.1 n=2	x̄ = 10.0 [8.8-11.4] σ = 0.7 n=26	x̄ = 9.3 [8.5-10.4] σ = 0.6 n=11	x̄ = 8.3 [7.0-9.8] σ = 0.7 n =131
	MD	--	8.9	--	x̄ = 9.6 [8.5-10.3] σ = 0.6 n=11	x̄ = 8.7 [7.7-9.9] σ = 0.8 n=7	x̄ = 9.3 [8.9-9.6] σ = 0.5 n=2	x̄ = 8.8 [7.0-10.0] σ = 0.6 n=24	x̄ = 8.4 [7.5-9.7] σ = 0.6 n=10	x̄ = 7.7 [6.2-8.8] σ = 0.5 n 122
P³	BL	--	11.6	--	x̄ = 11.7 [10.4-12.9] σ = 0.9 n=12	x̄ = 10.9 [10.5-12.1] σ = 1.5 n=7	--	x̄ =10.7 [9.1-11.9] σ = 0.8 n=30	x̄ =10.4 [10.0-11.1] σ = 0.4 n=10	x̄ = 9.4 [7.9-11.2] σ =0.7 n= 197
	MD	--	8.4	--	x̄ = 8.3 [7.4-9.1] σ =0.5 n=14	x̄ = 8.8 [8.0-10.7] σ = 0.9 n=7	--	x̄ = 8.0 [6.2-9.3] σ = 0.7 n=29	x̄ = 7.7 [7.0-8.7] σ = 0.6 n=10	x̄ = 7.1 [5.6-8.6] σ = 0.6 n=186
P⁴	BL	--	11.3	--	x̄ = 11.3 [9.9-13.4] σ = 0.9 n=22	x̄ = 11.1 [9.9-12.2] σ = 0.6 n=8	x̄ =11.3 - n=1	x̄ = 10.5 [8.2-11.7] σ = 0.7 n=25	x̄ = 10.4 [9.7-11.5] σ = 0.6 n=11	x̄ = 9.5 [7.6-12.3] σ = 0.8 n=194
	MD	--	8.3	--	x̄ = 8.1 [7.2-9.2] σ = 0.6 n=21	x̄ = 8.0 [7.3-8.4] σ = 0.4 n=7	x̄ = 7.9 - n=1	x̄ = 7.6 [5.7-8.8] σ = 0.9 n=25	x̄ = 7.1 [7.0-9.3] σ = 0.8 n=12	x̄ = 6.9 [5.4-11.3] σ = 0.8 n=173
M¹	BL	12.7	12.7	--	x̄ = 13.0 [11.7-14.7] σ = 0.9 n=18	x̄ = 12.1 [10.9-14.4] σ = 1.1 n=10	x̄ = 12.8 [11.8-13.8] σ = 1.0 n=3	x̄ = 12.2 [11.2-14.2] σ = 0.8 n=24	x̄ = 12.6 [11.2-15.2] σ = 1.3 n=22	x̄ = 11.5 [9.8-13.6] σ = 0.7 n=313
	MD	(12.1)	12.2	--	x̄ = 11.8 [10.0-13.6] σ = 0.9 n=21	x̄ = 11.5 [10.5-12.7] σ = 0.8 n=10	x̄ =12.4 [10.0-12.4] σ = 1.2 n=3	x̄ = 11.5 [8.5-13.6] σ = 1.1 n=22	x̄ = 11.5 [9.9-13.9] σ = 1.1 n=21	x̄ = 10.7 [8.7-13.3] σ = 0.7 n=279
M²	BL	12.3	12.4	13.8	x̄ = 13.3 [11.3-15.5] σ = 1.2 n=12	x̄ = 13.3 [11.3-16.3] σ = 1.3 n=10	x̄ = 12.5 [11.2-12.2] σ = 0.5 n=4	x̄ = 12.8 [11.2-16.2] σ = 1.1 n=25	x̄ = 12.3 [10.5-13.7] σ = 1.0 n=12	x̄ = 11.6 [9.1-14.1] σ =1.0 n= 229
	MD	10.9	11.8	12.6	x̄ = 11.6 [10.2-13.6] σ = 1.2 n=10	x̄ = 10.9 [9.7-12.4] σ = 0.9 n=9	x̄ = 11.1 [10.2-11.7] σ = 0.8 n=3	x̄ = 11.0 [9.3-13.1] σ = 1.1 n= 18	x̄ = 10.3 [8.6-11.8] σ = 0.8 n=9	x̄ = 9.9 [7.1-12.2] σ = 0.9 n= 199
M³	BL	--	12.4	13.3	x̄ = 12.2 [10.4-15.3] σ = 1.4 n=11	x̄ = 11.9 [10.1-13.3] σ = 1.0 n=7	x̄ = 11.5 [11.0-11.9] σ = 0.6 n=2	x̄ = 12.3 [8.6-14.2] σ = 1.3 n=19	x̄ = 11.7 [9.7-13.5] σ = 1.0 n=8	x̄ = 11.1 [7.6-14.4] σ = 1.2 n=129
	MD	--	8.4	11.6	x̄ = 10.0 [8.7-12.4] σ = 1.0 n=11	x̄ = 9.0 [8.0-11.0] σ = 0.9 n=7	x̄ = 10.0 [9.8-10.2] σ = 0.3 n=2	x̄ = 10.4 [8.4-13.9] σ = 1.1 n=19	x̄ = 9.3 [8.6-10.9] σ = 0.5 n=6	x̄ = 8.9 [6.1-12.8] σ = 1.1 n=115

Extended Data Table 3

|		Irhoud 3	Irhoud 11	*H. erectus*	MPE	MPAf	Neanderthals	EMH	RMH
I_1	BL	--	6.9	$\bar{x}=6.7$ [6.4-6.9] σ=0.2 n=3	$\bar{x}=6.9$ [6.4-7.5] σ=0.4 n=6	$\bar{x}=7.3$ [7.2-7.4] σ=0.2 n=2	$\bar{x}=7.4$ [6.8-8.2] σ=0.4 n=15	$\bar{x}=6.6$ [5.8-7.6] σ=0.6 n=10	$\bar{x}=5.8$ [4.8-6.8] σ=0.4 n=137
	MD	--	(5.8)	$\bar{x}=6.1$ [5.8-6.6] σ=0.4 n=3	$\bar{x}=5.7$ [4.9-7.5] σ=0.5 n=6	$\bar{x}=6.2$ [5.9-6.4] σ=0.4 n=2	$\bar{x}=5.5$ [4.3-6.3] σ=0.5 n=13	$\bar{x}=5.6$ [4.5-6.8] σ=0.9 n=10	$\bar{x}=5.4$ [4.2-6.8] σ=0.4 n=134
	RL	--	16.1	$\bar{x}=19.4$ - n=1	$\bar{x}=16.5$ - n=1	--	$\bar{x}=17.2$ [13.8-20.9] σ=1.9 n=17	$\bar{x}=14.4$ [13.7-16.6] σ=1.2 n=5	$\bar{x}=12.7$ [10.1-16.7] σ=1.5 n=39
I_2	BL	--	7.6	$\bar{x}=7.2$ [6.8-8.3] σ=0.7 n=4	$\bar{x}=7.5$ [6.7-8.6] σ=0.6 n=10	$\bar{x}=7.8$ - n=1	$\bar{x}=7.7$ [6.8-8.1] σ=0.3 n=17	$\bar{x}=7.1$ [6.4-8.0] σ=0.6 n=10	$\bar{x}=6.2$ [4.9-7.7] σ=0.5 n=146
	MD	--	(7.8)	$\bar{x}=7.4$ [7.2-7.9] σ=0.3 n=3	$\bar{x}=6.6$ [6.3-7.8] σ=0.4 n=10	$\bar{x}=7.4$ - n=1	$\bar{x}=6.5$ [5.2-7.5] σ=0.5 n=16	$\bar{x}=6.6$ [5.7-7.8] σ=0.7 n=9	$\bar{x}=6.0$ [5.0-6.8] σ=0.5 n=143
	RL	--	18.0	$\bar{x}=18.6$ [17.1-20.1] n=2	$\bar{x}=16.7$ - n=1	--	$\bar{x}=18.4$ [14.8-21.6] σ=2.0 n=15	$\bar{x}=15.4$ [13.7-17.3] σ=1.6 n=6	$\bar{x}=14.1$ [10.7-18.4] σ=1.4 n=47
C,	BL	9.1	9.4	$\bar{x}=8.8$ [8.3-9.6] σ=0.5 n=5	$\bar{x}=8.5$ [5.9-9.8] σ=1.1 n=11	$\bar{x}=8.8$ [7.7-10.0] σ=1.6 n=2	$\bar{x}=9.2$ [7.8-10.3] σ=0.7 n=24	$\bar{x}=8.6$ [7.0-10.2] σ=0.9 n=12	$\bar{x}=7.6$ [6.0-9.4] σ=0.7 n=132
	MD	9.1	8.6	$\bar{x}=8.4$ [8.0-8.9] σ=0.4 n=4	$\bar{x}=7.6$ [6.7-8.7] σ=0.5 n=11	$\bar{x}=7.8$ [7.2-8.4] σ=0.9 n=2	$\bar{x}=8.0$ [6.9-9.0] σ=0.5 n=22	$\bar{x}=8.2$ [6.4-10.0] σ=1.0 n=10	$\bar{x}=6.8$ [5.4-8.1] σ=0.5 n=124
	RL	--	20.6	--	$\bar{x}=20.8$ - n=1	--	$\bar{x}=20.7$ [16.1-25.6] σ=3.0 n=16	$\bar{x}=17.8$ [16.1-19.8] σ=1.3 n=6	$\bar{x}=16.6$ [13.2-19.2] σ=1.8 n=23
P_3	BL	10.2	9.6	$\bar{x}=10.3$ [8.9-11.5] σ=0.9 n=11	$\bar{x}=9.0$ [8.4-10.0] σ=0.3 n=9	$\bar{x}=9.7$ [9.4-10.0] σ=0.4 n=2	$\bar{x}=9.1$ [7.2-10.3] σ=0.7 n=31	$\bar{x}=9.1$ [8.0-12.2] σ=1.2 n=10	$\bar{x}=8.0$ [6.4-10.2] σ=0.7 n=173
	MD	9.7	9.2	$\bar{x}=8.8$ [7.9-9.9] σ=0.6 n=11	$\bar{x}=7.9$ [7.4-8.4] σ=0.3 n=8	$\bar{x}=9.4$ [8.8-10.0] σ=0.9 n=2	$\bar{x}=8.0$ [6.3-9.9] σ=0.7 n=31	$\bar{x}=8.2$ [7.2-11.0] σ=1.1 n=9	$\bar{x}=7.1$ [5.8-8.6] σ=0.6 n=160
P_4	BL	10.5	10.5	$\bar{x}=10.6$ [9.6-11.7] σ=0.7 n=12	$\bar{x}=8.6$ [7.2-10.1] σ=0.9 n=11	$\bar{x}=9.9$ [8.7-11.1] σ=0.9 n=5	$\bar{x}=9.3$ [7.6-11.1] σ=0.8 n=28	$\bar{x}=9.3$ [7.8-10.9] σ=0.9 n=16	$\bar{x}=8.4$ [6.8-10.8] σ=0.7 n=165
	MD	9.5	8.9	$\bar{x}=8.7$ [7.2-9.9] σ=0.8 n=9	$\bar{x}=7.4$ [6.6-9.5] σ=0.8 n=11	$\bar{x}=8.9$ [7.5-10.3] σ=0.9 n=6	$\bar{x}=7.9$ [5.7-11.8] σ=1.2 n=23	$\bar{x}=7.8$ [7.0-9.6] σ=0.9 n=12	$\bar{x}=7.2$ [5.6-10.4] σ=0.7 n=151
M_1	BL	12.3	12.2	$\bar{x}=12.2$ [10.7-13.5] σ=0.8 n=15	$\bar{x}=10.6$ [9.7-11.5] σ=0.6 n=15	$\bar{x}=11.7$ [10.5-12.6] σ=0.7 n=7	$\bar{x}=11.1$ [9.7-12.9] σ=0.7 n=36	$\bar{x}=11.7$ [10.5-14.3] σ=1.0 n=19	$\bar{x}=10.7$ [8.6-12.6] σ=0.7 n=267
	MD	14.5	12.5	$\bar{x}=13.3$ [12.1-14.9] σ=1.0 n=13	$\bar{x}=11.2$ [10.6-12.0] σ=0.5 n=16	$\bar{x}=12.8$ [11.9-13.8] σ=0.7 n=8	$\bar{x}=11.8$ [10.1-13.6] σ=0.9 n=33	$\bar{x}=12.6$ [10.8-14.2] σ=1.0 n=20	$\bar{x}=11.4$ [9.2-13.5] σ=0.7 n=243
M_2	BL	12.2	12.2	$\bar{x}=13.1$ [11.7-14.3] σ=0.8 n=14	$\bar{x}=10.4$ [8.6-12.4] σ=0.9 n=17	$\bar{x}=11.5$ [10.3-12.9] σ=0.9 n=6	$\bar{x}=11.1$ [9.6-12.4] σ=0.7 n=32	$\bar{x}=11.0$ [9.2-12.7] σ=1.0 n=22	$\bar{x}=10.4$ [8.6-12.5] σ=0.8 n=207
	MD	(15.3)	13.0	$\bar{x}=13.3$ [12.5-14.4] σ=0.6 n=12	$\bar{x}=11.5$ [9.7-14.8] σ=1.3 n=17	$\bar{x}=12.8$ [12.0-13.8] σ=0.7 n=6	$\bar{x}=12.0$ [10.5-14.0] σ=0.9 n=29	$\bar{x}=11.7$ [10.2-14.2] σ=1.1 n=15	$\bar{x}=10.9$ [8.9-14.3] σ=0.9 n=198
M_3	BL	--	11.1	$\bar{x}=12.4$ [11.0-14.2] σ=0.9 n=7	$\bar{x}=10$ [8.7-11.3] σ=0.8 n=10	$\bar{x}=11.4$ [10.6-12.3] σ=0.6 n=5	$\bar{x}=10.8$ [7.9-13.1] σ=0.8 n=29	$\bar{x}=10.8$ [9.2-12.8] σ=1.0 n=14	$\bar{x}=10.4$ [8.6-12.6] σ=0.8 n=139
	MD	--	12.8	$\bar{x}=12.8$ [10.9-14.7] σ=1.3 n=6	$\bar{x}=11.2$ [9.4-12.7] σ=0.9 n=10	$\bar{x}=13.3$ [12.3-15.2] σ=1.3 n=4	$\bar{x}=11.8$ [9.4-13.9] σ=0.9 n=26	$\bar{x}=11.8$ [10.1-13.8] σ=1.1 n=14	$\bar{x}=10.8$ [8.2-12.6] σ=1.0 n=119

Extended Data Table 4

Lower Dentition	Irhoud 3, 11	*H. erectus*	MPE	MPAf	Neanderthals	EMH	RMH
P$_4$ Lingual Cusps [pres. >1]	50 (2)	85.7 (7)	50 (4)	50 (2)	97 (31)	71.4 (7)	66.7 (173)
P$_4$ Metaconid position [pres = mesial]	100 (2)	90.9 (11)	100 (5)	66.7 (3)	97 (32)	62.5 (8)	80.6 (177)
P$_4$ Transverse Crest [pres. >0]	0 (2)	36.4 (11)	40 (5)	75 (4)	90 (31)	12.5 (8)	4.5 (177)
P$_4$ Distal Accessory Ridge [pres. >0]	50 (2)	75 (8)	100 (3)	100 (2)	87 (15)	66.7 (3)	47.1 (145)
P$_4$ Mesial Accessory Ridge [pres. >0]	0 (2)	0 (7)	25 (4)	100 (2)	13 (25)	66.7 (3)	29.5 (152)
P$_4$ Asymmetry [pres >0]	100 (2)	46.2 (13)	20 (5)	66.7 (3)	95 (20)	37.5 (8)	0.8 (119)
P$_4$ Fissure Pattern [pres. = U]	0 (2)	0 (5)	0 (3)	0 (2)	0 (14)	75 (4)	72.9 (145)
M$_1$ Middle Trigonid Crest [pres. >0]	0 (2)	33.3 (12)	88.9 (11)	50 (2)	92.9 (28)	35.7 (14)	1.4 (207)
M$_1$ Protostylid [pres.>2]	50 (2)	50 (8)	0 (9)	33.3 (3)	0 (38)	11.8 (17)	0.5 (218)
M$_1$ Cusp 6 [pres. >0]	100 (2)	28.6 (7)	33.3 (6)	100 (1)	38 (21)	0 (12)	18.1 (200)
M$_1$ Cusp 7 [pres. >0]	100 (2)	50 (12)	12.5 (8)	0 (2)	18 (33)	45.0 (20)	9.7 (236)
M$_2$ Y Groove Pattern [pres. = Y]	50 (2)	91.7 (12)	57.1 (7)	0 (1)	79 (33)	76.9 (13)	28.6 (242)
M$_2$ Cusp number [pres.= 4]	0 (2)	0 (13)	0 (7)	0 (3)	0 (37)	11.8 (17)	63.8 (242)

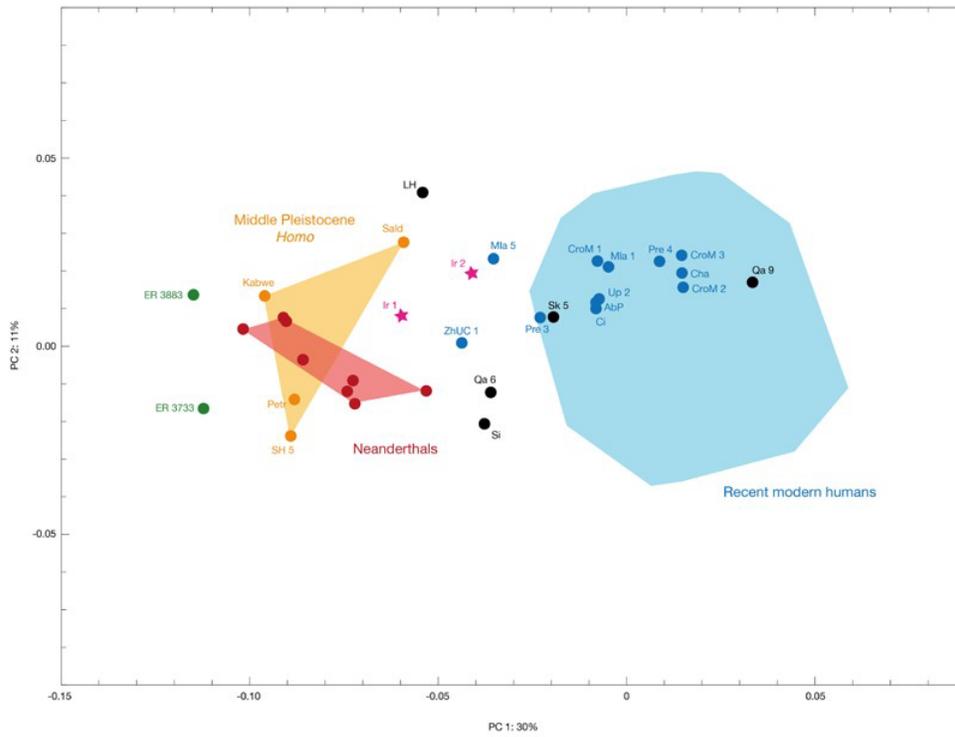| Upper Dentition	Irhoud 10, 21, 22	*H. erectus*	MPE	MPAf	Neanderthals	EMH	RMH
I^2 Shoveling [pres >1]	Present (1)	100 (3)	--	100 (1)	100 (15)	83.3 (6)	23.2 (122)
I^2 Tuberculum dentale [pres >1]	Present (1)	0 (2)	--	100 (1)	88.9 (9)	60 (5)	38.1 (118)
C Distal Accessory Ridge [pres. >0]	Present (1)	66.7 (3)	--	100 (1)	62.5 (8)	100 (2)	39.7 (68)
M^2 Metacone Reduction [pres. <3.5]	0 (2)	0 (8)	0 (4)	0 (1)	5.9 (34)	0 (10)	18.3 (243)
M^2 Hypocone Reduction [pres. <3]	0 (2)	0 (8)	0 (4)	0 (1)	2.9 (34)	0 (8)	24.5 (241)
M^1 Cusp 5 [pres. >0]	Present (1)	0 (2)	67.7 (3)	100 (1)	63.6 (22)	50 (10)	41.2 (232)
M^1 Carabelli's Trait [pres. >2]		0 (2)	33.3 (3)	0 (1)	72 (25)	50 (10)	46.2 (272)
M^1 Parastyle [pres. >0]	Absent (2)	0 (1)	0 (2)	0 (1)	20.8 (24)	0 (14)	0.8 (299)
M^1 Mesial Accessory Cusps [pres >0]	Absent (1)	--	0 (2)	--	45.4 (11)	100 (2)	67.1 (132)

Extended Data Table 5
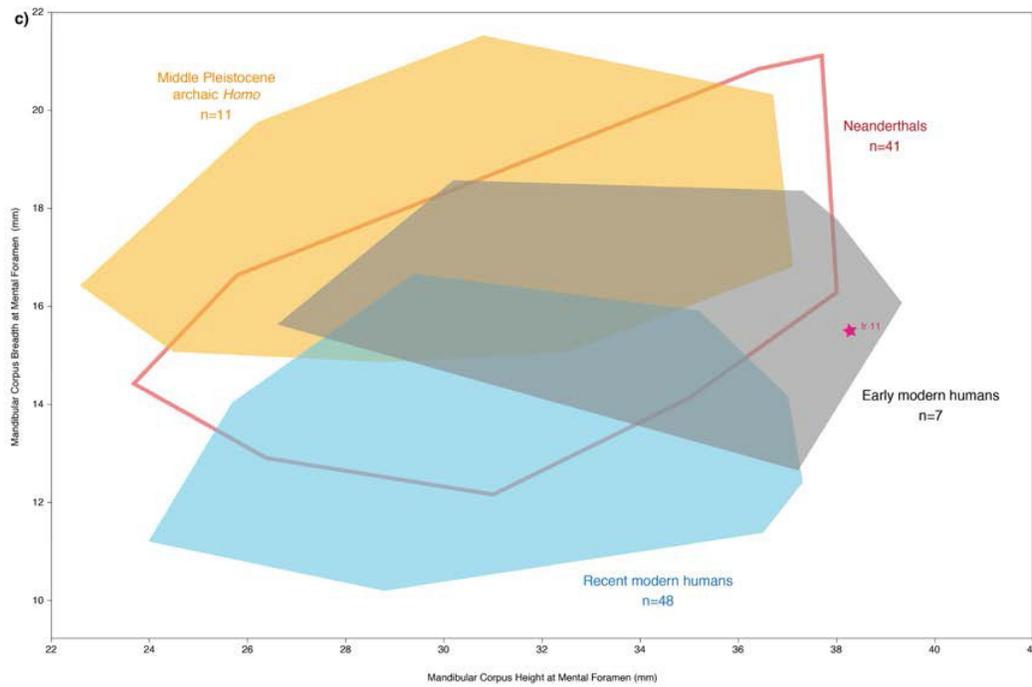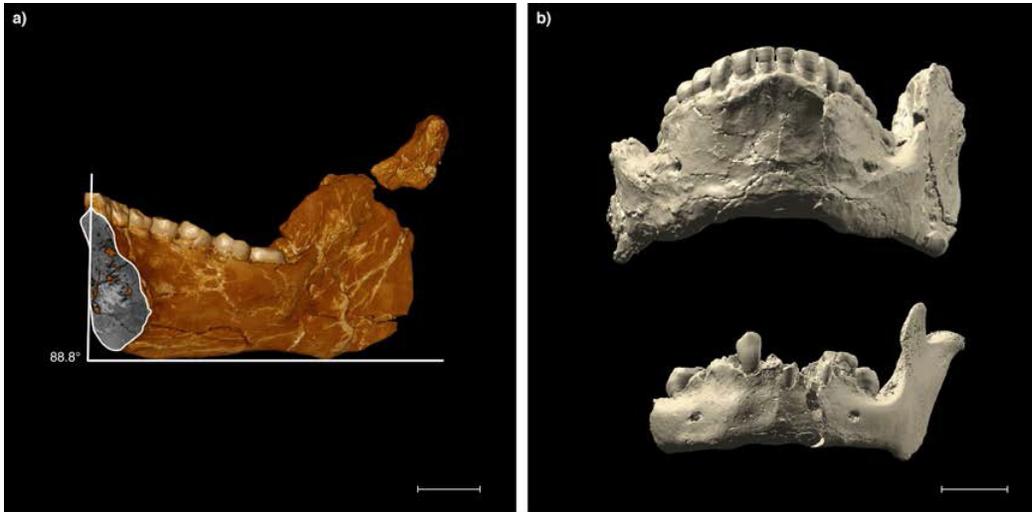
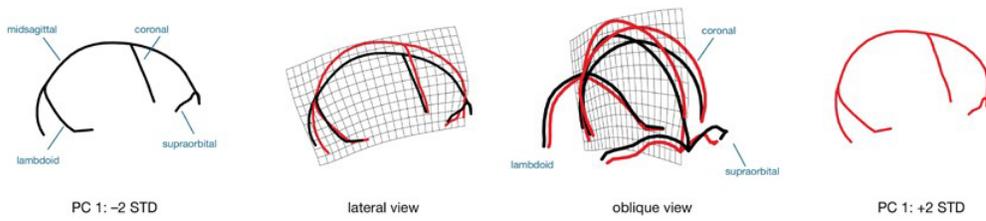**Extended Data Figure 1**
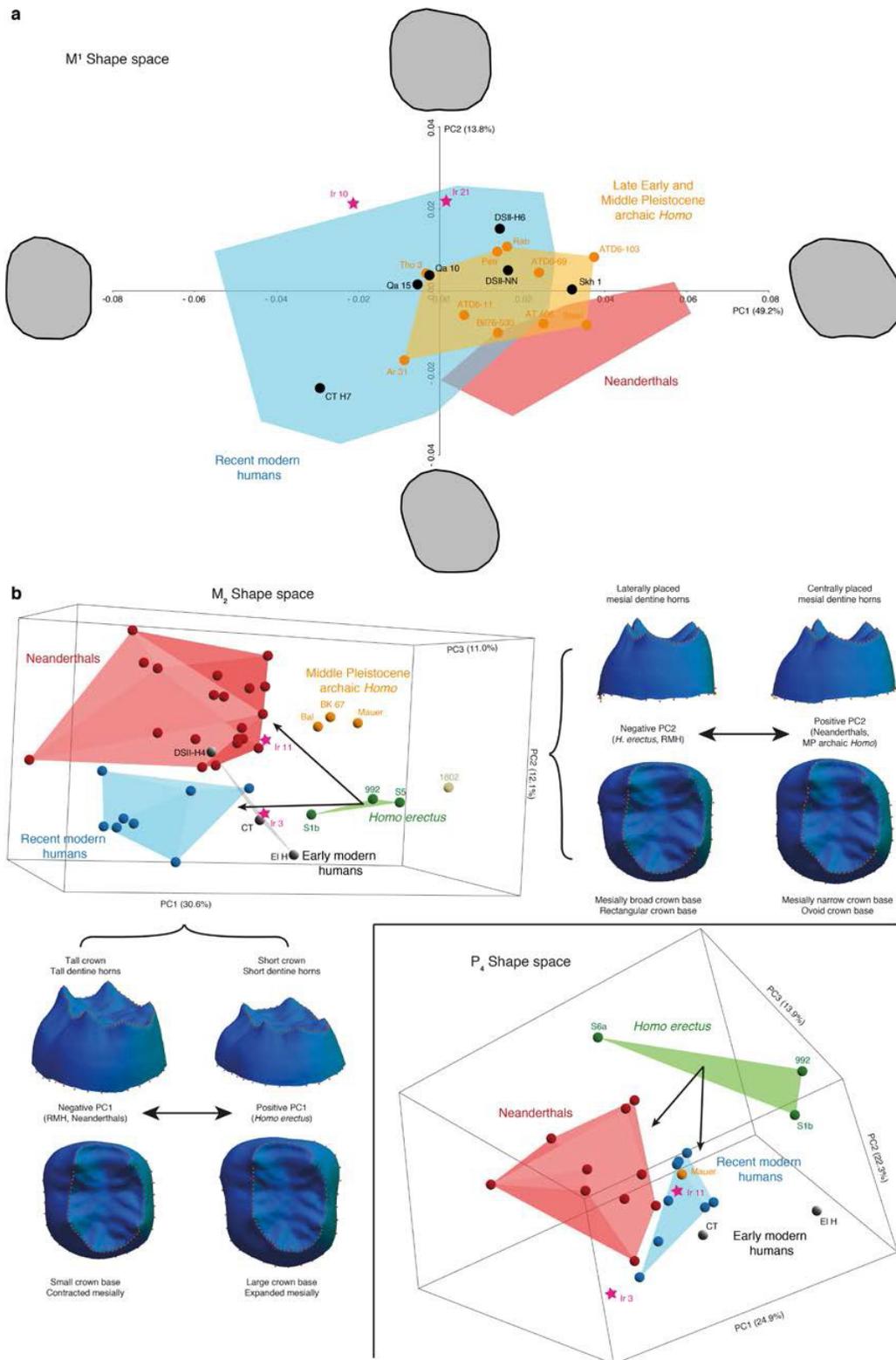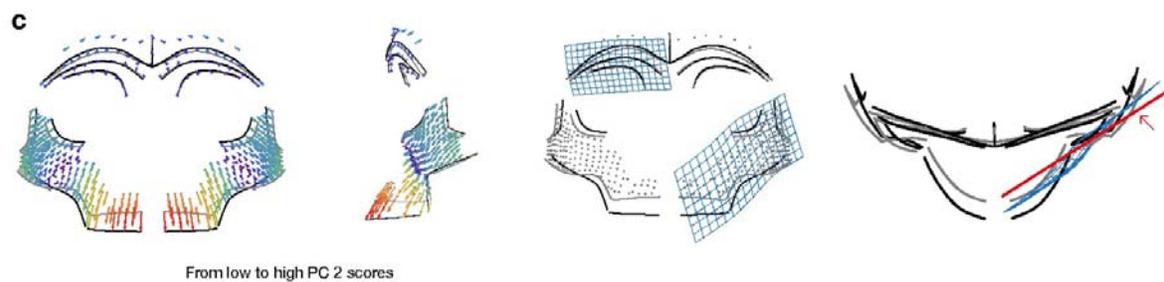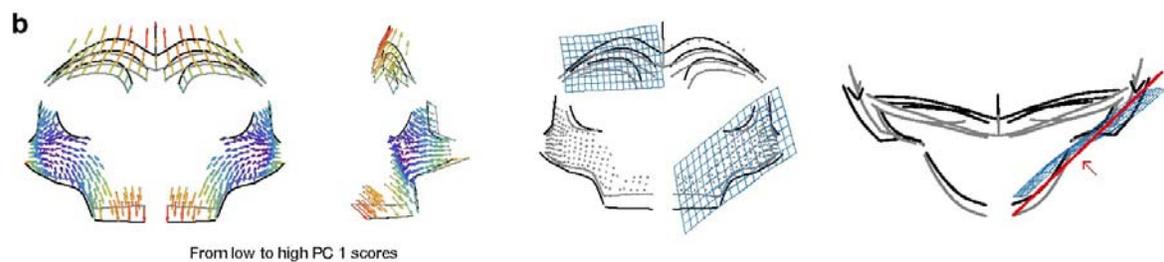
Extended Data Figure 2
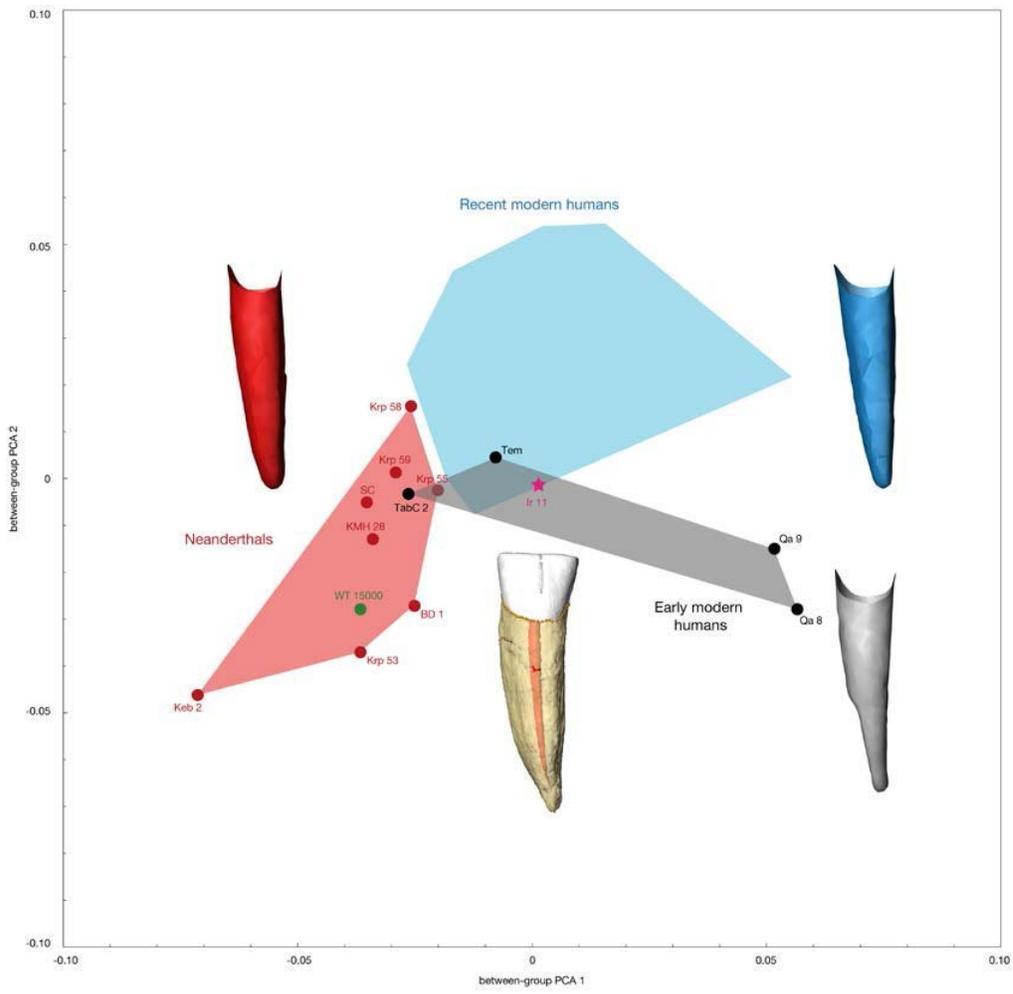
Extended Data Figure 3

a Principal component analysis: Shape of the external vault

b

PC 1: –2 STD   lateral view   oblique view   PC 1: +2 STD

Extended Data Figure 4

a

recent *Homo sapiens*

Neanderthal to *H. sapiens* H. sapiens to Neanderthal

H. erectus to *H. sapiens* H. sapiens to *H. erectus*

Neanderthal to *H. erectus*

Neanderthals

Homo erectus

H. erectus to Neanderthal

b

From low to high PC 1 scores

c

From low to high PC 2 scores

Extended Data Figure 5